Minimal Microscopic Model for the Contraction of Stress Fibres

Written by Emma Comino under the supervision of Dietmar Oelz
November 7, 2022

Abstract

Stress fibres are contractile filament bundles in many non-muscle cells. Consisting of polarised actin filaments, myosin motors and cross-linking proteins, these components work together to facilitate cell movement. However, the network structure of stress fibres in many cell types is relatively random, and it is not well understood what asymmetries are present that could cause contractile behaviours to be favoured over expansive. We propose an overdamped one-dimensional particle model for actin filaments and myosin motor proteins. This allows us to computationally explore a minimal model for contraction, by which myosin slides off rapidly when approaching the plus ends of actin filaments.

Acknowledgements

None of this thesis would have been possible without the creativity and patience of my supervisor. Thank you Dietmar for sharing your wonderful area of mathematics with me as well as your coding tips and tricks to help me design and build a working model. Thank you friends and family for putting up with me whilst I slugged through the write up, and struggled to articulate my ideas. I think this year has shown me plenty, and I am glad for it. I hope you enjoy reading.

Contents

1 Introduction

Stress fibres allow a variety of different cells to move [2, 1, 20]. Consisting of dense bundles of microscopic filaments, it is difficult to visualise how stress fibres contract and hence facilitate this movement [22, 17]. Many have theorised potential mechanisms that could induce contraction, such as filaments buckling, flexing or treadmilling [16, 21, 19], however these explanations are complex and difficult to verify experimentally. In this thesis, we present a one-dimensional mechanism that is equivalent to a two-dimensional motion proposed in *F-Actin Bending Facilitates Net Actomyosin Contraction By Inhibiting Expansion With Plus-End-Located Myosin Motors* [21]. We construct an energy functional, describing how a stress fibre's components interact, and utilise it to simulate stress fibre contractility. As a result of our investigation, we determine that the mechanism does generate contraction in our model, providing a simplistic explanation that could be verified macroscopically.

2 Background

2.1 Stress Fibres

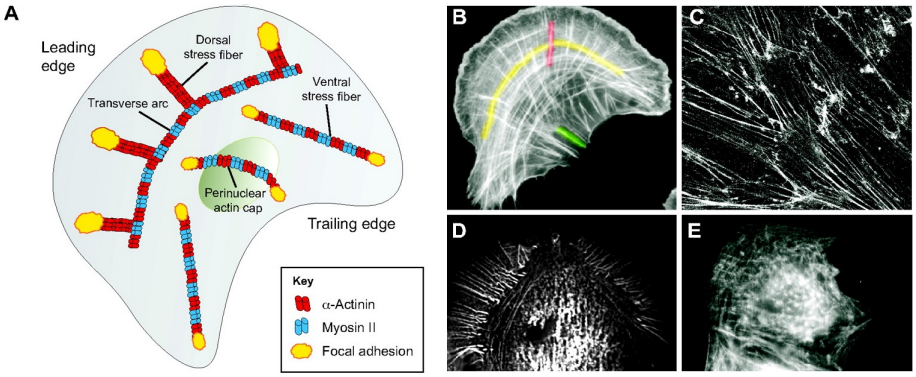

Figure 1: Different types of stress fibers in cultured animal cells [24]

Stress fibres (Figure 1) are contractile structures that are found in many non-muscle cells [24]. Some of these cells include:

- Fibroblast cells, which play important roles in wound healing such as creating scaffolding for tissue regeneration and shrinking scars [2],
- Endothelial cells, which line blood vessels facilitating cell migration for tissue growth and repair [1], and
- Epithelial cells, which protect an organism from its environment and make up skin, lung lining, etc. [20].

Stress fibres allow these cells to contract, pull themselves along, and hence move. However, unlike in muscle cells (Figure 2a), the contraction of stress fibres in non-muscle cells (Figure 2b) is not well understood. Whilst striated muscle cells consist of sarcomeres, an ordered network of actomyosin whereby clusters of motors can bind to bundles of actin filaments and slide along them for a long time [14], the stress fibres in non-muscle cells have been observed to contract, despite lacking the sarcomeric network organisation to induce contraction [22]. As a result, it is unclear how a disordered stress fibre network could still induce a contractile force [17], and we would like to understand how stress fibres contract to facilitate these cells' functions.

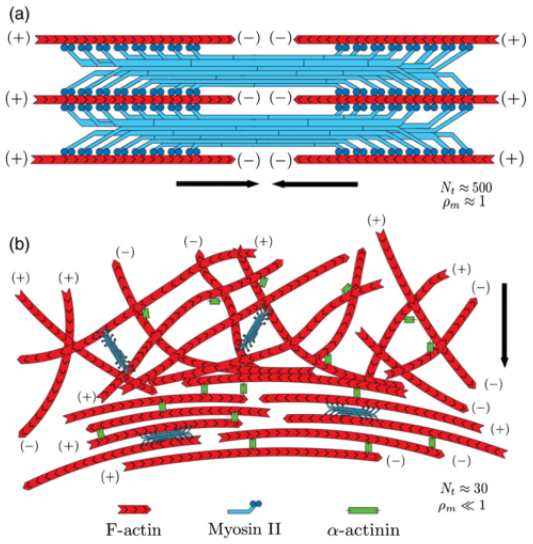

Figure 2: Actomyosin networks in (a) muscle cells and (b) non-muscle cells [13]

Stress fibres consist of actomyosin networks (see Figure 2b), which are composed of bundles of polarised actin filaments and myosin motors [24]. These motors connect to filaments and move to their barbed (plus) end [17]. Cross-linking proteins that bind to filaments and inhibit their movement are also present [24, 3]. Additionally, focal adhesions are the point of contact where the stress fibre grabs onto the cell's external environment (see Figure 1a) [5]. As a result, whilst we know what components may factor into stress fibre contraction, their disorder makes it unclear what structural biases exist to facilitate contraction rather than equally favour contraction and expansion [3, 17].

Modelling stress fibres then requires understanding of several mathematical techniques. In particular, stress fibres are moving through the cell's cytoplasm, which is a thick fluid. The viscosity of the cytoplasm will impose friction on the stress fibre, slowing its movement. Therefore, the system can be thought of as an isotropic linear viscoelastic material [25], meaning that a Kelvin-Voigt model can been used to define the force-balance equations describing it.

If we consider first the damped oscillator presented in Figure 3, the displacement $u(t)$ of the mass away from its equilibrium position can be described by

$$\underbrace{m\frac{\mathrm{d}^2u}{\mathrm{d}t^2}}_{\substack{\text{Inertial}\\ \text{force}}} + \underbrace{c\frac{\mathrm{d}u}{\mathrm{d}t}}_{\substack{\text{Damping}\\ \text{force}}} + \underbrace{ku}_{\substack{\text{Restoring}\\ \text{force}}} = 0,$$

from Newton's second law [12]. In our biological context, masses are very small, meaning that inertial forces are negligible as compared to the other forces, and we neglect them as a result,

$$c\frac{\mathrm{d}u}{\mathrm{d}t} + ku = 0.$$

We refer to this movement as overdamped dynamics. Moreover, if we have additional components and sources of friction, we can introduce more ordinary differential equations. Since these equations will depend on each other, they are coupled, and will form the force balance equations describing the behaviour of the entire system. In Section 3, we describe how we derived our system containing

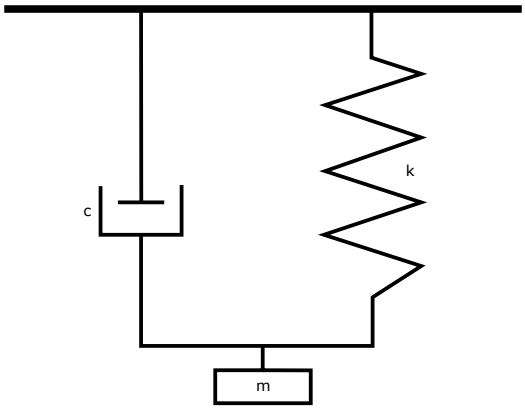

Figure 3: A viscoelastic system consisting of a mass m connected to a dashpot (with associated damping coefficient c) and a spring (with spring constant k) acting in parallel. If the mass is pulled from its equilibrium length, the spring will oscillate compressing and stretching, whilst the friction caused by the dashpot slows movement. This friction causes the oscillations to weaken, or dampen, until the spring returns to rest at its equilibrium length. This damped oscillator is also called a Kelvin-Voigt element [12].

the equations that describe

$$\begin{cases} N \text{ actin filaments} \\ M \text{ myosin motors, and} \\ 2 \text{ focal adhesions.} \end{cases}$$

Computationally, we can solve such a system using an implicit Euler scheme [4]. More specifically, we can discretise time into steps Δt and describe the (discrete) derivative of the solution u_n, where $n \in \mathbb{N}_0$, as the negative gradient of a potential Φ, i.e.

$$-\Phi'(u_{n+1}) = \frac{u_{n+1} - u_n}{\Delta t}.$$

If we rearrange this as follows,

$$0 = \frac{u_{n+1} - u_n}{\Delta t} + \Phi'(u_{n+1}),$$

we recall that, to find a minimiser, we set the function's derivative to zero. Therefore, solving the above problem for u_{n+1} is equivalent to determining

$$u_{n+1} = \underset{u}{\operatorname{argmin}} \left\{ \frac{(u - u_n)^2}{2\Delta t} + \Phi(u) \right\}.$$

Many optimisation techniques exist for numerically solving this problem, including simulated annealing and gradient descent. For our numerical scheme, we use LBFGS, which is a fast, low storage method for nonlinear optimisation [18]. Automatic differentiation was then used to approximate the gradient, which is required by the optimisation method [18].

If we introduce new components into the system, this may affect how the material will displace. So, we will now think of each new u iterate as a different displacement function that changes as a result of other components moving in the system concurrently. We then call the expression inside the curly

braces an energy functional E. It is a functional because, instead of accepting values, it takes in a function. We notate the input of a functional with square parentheses, as demonstrated below.

$$E[u] = \frac{(u - u_n)^2}{2\Delta t} + \Phi(u)$$

Energy then refers to the capacity of doing work [8]. In our application, the energy functional includes potential energy, describing the energy stored in the system as a result of its position [7]. For example, if an elastic band is held taut, it has elastic potential energy because, once it is let go, the elastic band snaps back and the energy is released. Additionally, the energy functional contains dissipative terms mimicking friction. These terms are included in the energy such that the minimisation scheme will penalise excessive movement. More specifically, in the frictional term $(u - u_n)^2/(2\Delta t)$, if the new displacement u is very different to the previous u_n, then the energy required will be greater. As a result, the system will try to keep u close to u_n, so there is resistance to movement, and hence friction. This relates to nature, like how water rolling down a hill will travel in the direction of least resistance. You may note the energy functional is a Hamiltonian but without kinetic energy terms, since these are inertial and relate to the mass.

However, now we have a functional to minimise. We recall that setting the gradient $\boldsymbol{\nabla} f = (\frac{\mathrm{d}f}{\mathrm{d}x_1}, \frac{\mathrm{d}f}{\mathrm{d}x_2}, \ldots, \frac{\mathrm{d}f}{\mathrm{d}x_n})$ to $\vec{0}$ allows us to determine the location of critical points. In our setting, functional (variational) derivatives are the analogous [9]. For our purposes, we define this as

$$\delta E = \lim_{\epsilon \to 0} \frac{E[u + \epsilon\delta_u] - E[u]}{\epsilon}$$

where δ_u is an arbitrary function perturbing u, and call it the variation [10].

2.2 Literature Review

Myosin motors move towards the plus end of attached filaments, but this does not generate a bias towards contraction, since the motors' positions are randomised and can cause expansion and contraction equally. To elaborate, if we consider a (blue) myosin motor attached to two actin filaments (red) like in Figure 4, the motor will walk to the filaments plus ends, pulling them together and causing the stress fibre to contract. However, if this attraction to the plus end continues, the motor would eventually repel the filaments, causing the stress fibre to expand. This is precisely the behaviour described in *Geometrical Origins of Contractility in Disordered Actomyosin Networks* [14], where the microscopic components of the network exhibit both expansive and contractile behaviours locally. As such, there must exist a mechanism that breaks this symmetry such that the overall stress fibre favours contractile behaviours [17].

Many mechanisms have been explored mathematically to explain the contraction bias in disordered actomyosin networks. For example, Lenz et al. (2012) suggested filament buckling [16], whereby the length of filaments reduced in response to longitudinal forces (see Figure 5a). The buckling would prevent expansive motions, and hence improve contractility. Lenz (2014) later extended this idea to higher dimensions, identifying an additional three contractile mechanisms [14]. In this new model, it was found that a fixed-sized motor could induce contraction instead. The motor connected to two cross-linked filaments would cause the filaments to rotate to be more parallel in a "closing the zipper" motion, generating a contractile force (see Figure 5b).

In vivo experiments have also indicated that the force generated by actomyosin networks is dependent on actin turnover [23]. Turnover, as a means of generating contraction, was simulated and explored in the paper, *Role of Turnover in Active Stress Generation in a Filament Network* [11]. Hiraiwa et al. (2016) investigated the behaviour of a 2D model where passive cross-linkers and fast motors constrained rigid polarised filaments at a point, allowing the filaments to freely

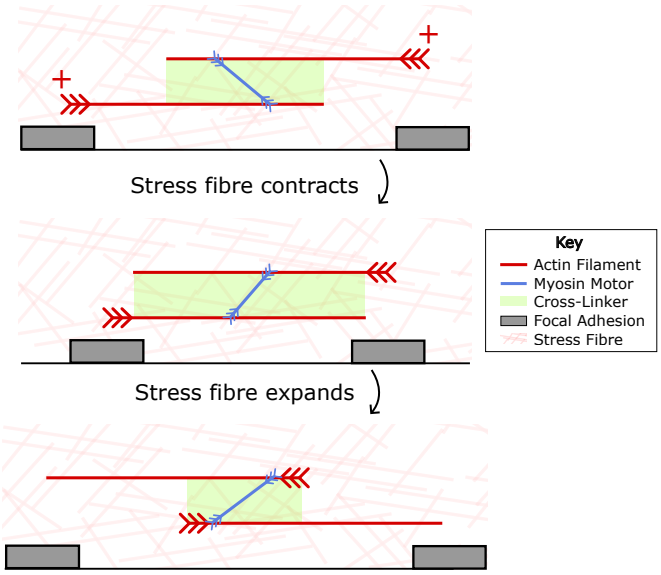

Figure 4: Interaction between actin filaments and myosin motor. These components exhibit both expansive and contractile behaviours [14].

rotate. Motors and cross-linkers could then turn over from a reservoir of inactive components, with turnover occurring over a slower time-scale than motor movement (see Figure 5c). Hiraiwa et al. identified that contraction occurs in their model when an appropriate ratio between cross-linker and filament turnover was chosen. This was because fast filament turnover prevented motors exerting a force, whereas fast cross-linker turnover formed clusters, breaking the stress fibre. So, if filament and cross-linker turnover were appropriately balanced, the frequency of expansive behaviours was reduced, and hence contraction occurred [11]. As a result, turnover was introduced into our model (Section 4.4) to verify whether it could have the same effect in 1D.

On the other hand, Lenz et al. (2012) in *Requirements for contractility in disordered cytoskeletal bundles* ignored motors and cross-linkers changing attachments [15]. Instead they made several assumptions, such as a motor's velocity being impacted by the force an attached filament exerts on it, the deformation of a filament depends on forces applied longitudinally at its ends, and the filament bundle does not undergo polarity sorting. On average, they found that bundles composed of rigid filaments contract if the filaments display nonlinear elastic behaviour [15]. We investigate the nonlinearity of our model in Section 4.1.

In the paper *F-Actin Bending Facilitates Net Actomyosin Contraction By Inhibiting Expansion With Plus-End-Located Myosin Motors*, Tam et al. (2022) developed a PDE model for two semi-flexible actin filaments with an attached myosin motor [21]. The two-dimensional model used a plane stress tensor as a measure for contractility, and showed that rigid filaments expanded and contracted symmetrically. When the filaments could bend, it introduced an asymmetry whereby the motor could slide off faster as it approached the filaments' plus ends. This was because the filaments could deform such that they were closer together, which reduced the force opposing the motor's movement (see Figure 5d). The fast motor slide-off reduced expansive behaviours and hence the system favoured contraction. Considering flexible filaments was unlike all aforementioned papers, and we wanted to replicate a similar behaviour except in 1D. We propose early motor drop-offs (introduced in Section 4.2) as a feature in our model to replicate the 2D flexible filament model whilst simplifying it to 1D. We believe if we can create a more concise explanation for stress fibre

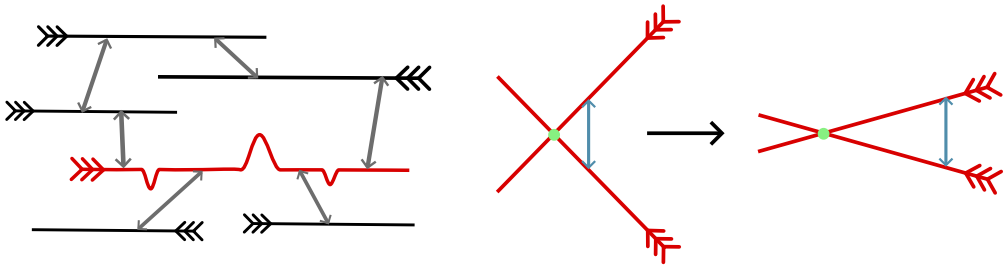

(a) 1D filament buckling as proposed in [16]. Buckled filament highlighted in red.

(b) 2D fixed sized motor as proposed in [14].

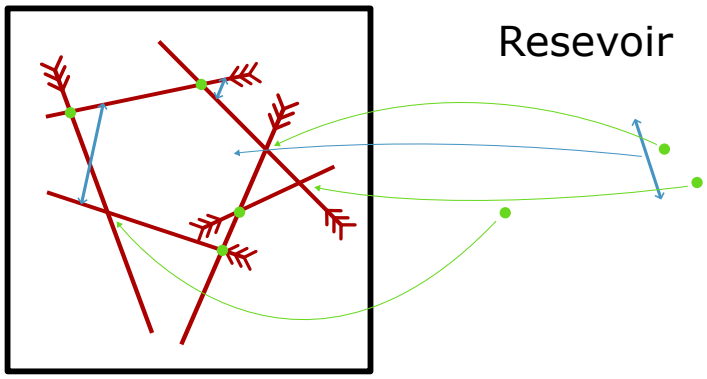

(c) 2D cross-linker and motor turnover as proposed in [11].

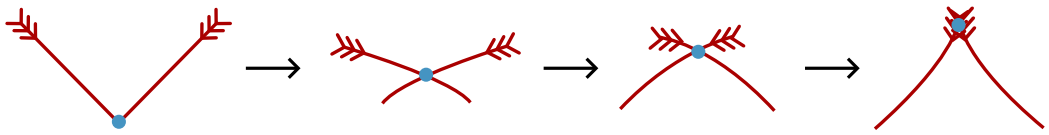

(d) 2D semi-flexible filaments as proposed in [21].

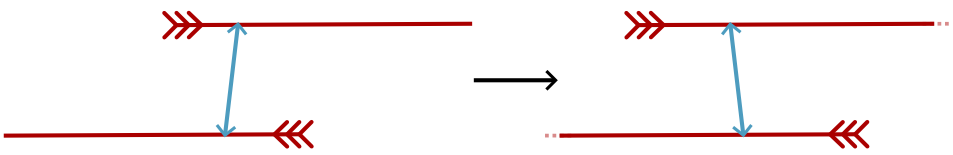

(e) 1D filament treadmilling. This mechanism is proposed in a ring in [19].

Figure 5: Various mechanisms theorised to induce contraction in stress fibres. Filaments are red with barbs depicting their plus end, motors are blue and cross-linkers are green.

contraction, then the minimal model (with fewer moving parts) can be explained by experimental results.

As for developing a computational model, energy minimisation is a technique commonly used in mathematical biology. For example, the semi-flexible filament model relies on curve-straightening flow, whereby filaments tend to minimise bending as it requires more energy [21]. Moreover, in *A Combination of Actin Treadmilling and Cross-Linking Drives Contraction of Random Actomyosin Arrays*, Oelz et al. (2015) present an energy minimisation scheme on a ring geometry, theorising that, in order to contract, the circularly bundled filaments undergo treadmilling, whereby their plus ends lengthen whilst their minus ends shorten (see Figure 5e) [19]. As such, it makes sense to employ energy minimisation instead on a line geometry, presented in the coming section.

3 Mathematical Model

To computationally investigate the contractile behaviours of a stress fibre, we first realise the structure as an interval of overlapping actin filaments and connected myosin motors (see Figure 6). The centre positions of the red actin filaments are stored on a number line which, in the figure, we have visualised spread above the interval (black). Their overlap, depicted in green, represents cross-linking proteins, and the blue arrows indicate the myosin motors that are connected to two filaments. As time progresses, these motors will crawl to the plus (barbed) ends of the connected filaments. Focal adhesions are illustrated as grey intervals at either end of the stress fibre. They overlap the edge actin filaments.

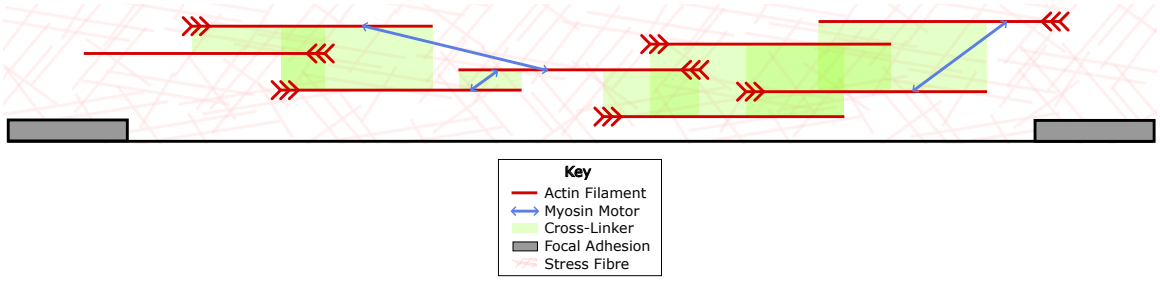

Figure 6: One dimensional interpretation of a stress fibre.

The degrees of freedom of our model include the centre positions of N actin filaments at time $n = 1, 2, \ldots, T$, given by

$$\mathbf{x}^n = (x_1^n,\, x_2^n,\, \ldots,\, x_N^n),$$

as well as the centre position of M myosin motors

$$\mathbf{y}^n = (y_1^n, y_2^n,\, \ldots,\, y_M^n),$$

and the centre position of the interval's end points

$$\mathbf{z}^n = (z_A^n, z_B^n).$$

Our model relies on overdamped dynamics formulated as a steepest descent scheme,

$$\left(\mathbf{x}^{n+1},\, \mathbf{y}^{n+1},\, \mathbf{z}^{n+1}\right) = \underset{\substack{\mathbf{x}\in\mathbb{R}^N \\ \mathbf{y}\in\mathbb{R}^M \\ \mathbf{z}\in\mathbb{R}^2}}{\operatorname{argmin}} E[\mathbf{x}, \mathbf{y}, \mathbf{z}], \tag{1}$$

associated to an energy functional of the following structure,

$$E[\mathbf{x},\mathbf{y},\mathbf{z}] = \underbrace{E_f[\mathbf{x}]}_{\substack{\text{Actin}\\ \text{Filaments}}} + \underbrace{E_m[\mathbf{x},\mathbf{y}]}_{\substack{\text{Myosin}\\ \text{Motors}}} + \underbrace{E_a[\mathbf{x},\mathbf{z}]}_{\substack{\text{Focal}\\ \text{Adhesions}}}. \tag{2}$$

In this section, we derive the energy functional's (Equation 2) corresponding force balance equations and describe how they may capture important mechanisms in the stress fibre's structure. We achieve this by computing the variation of the energy functional, passing it to the limit where the time step Δt becomes small, before ensuring the result is equal to zero, where extremal values occur.

3.1 Actin Filaments

The first component of Equation 2 describes the behaviours of the actin filaments if they were to act alone. It is defined as

$$E_f[\mathbf{x}] = \xi \sum_{i=1}^{N} \frac{(x_i - x_i^n)^2}{2\Delta t} + \eta \sum_{i=1}^{N}\sum_{j=1}^{N} \frac{O_{ij}}{2} \frac{\left(x_i - x_j - (x_i^n - x_j^n)\right)^2}{2\Delta t}, \tag{3}$$

where $O \in \mathbb{M}^{N\times N}$ is a symmetric matrix with each element representing the distance by which two different filaments i and j of length l are overlapping, i.e.

$$O_{ij} = \begin{cases} \max\{l - |x_i - x_j|, 0\} & \text{if } i \neq j, \\ 0 & \text{if } i = j. \end{cases}$$

Computing the total variation of Equation 3, we obtain

$$\begin{aligned}\delta E_f[\mathbf{x}] = \xi \sum_{i=1}^{N} \frac{x_i - x_i^n}{\Delta t}\delta_{x_i} + \eta \sum_{i=1}^{N}\sum_{j=1}^{N} \frac{O_{ij}}{2} \frac{x_i - x_j - (x_i^n - x_j^n)}{\Delta t}\delta_{x_i} \\ - \eta \sum_{i=1}^{N}\sum_{j=1}^{N} \frac{O_{ij}}{2} \frac{x_i - x_j - (x_i^n - x_j^n)}{\Delta t}\delta_{x_j},\end{aligned}$$

where δ_{x_i} is a small perturbation of x_i. In the final term, since it was arbitrary which order we took the double sum, we can rewrite it as

$$-\eta \sum_{j=1}^{N}\sum_{i=1}^{N} \frac{O_{ji}}{2} \frac{x_j - x_i - (x_j^n - x_i^n)}{\Delta t}\delta_{x_i},$$

and hence

$$\delta E_f[\mathbf{x}] = \xi \sum_{i=1}^{N} \frac{x_i - x_i^n}{\Delta t}\delta_{x_i} + \eta \sum_{i=1}^{N}\sum_{j=1}^{N} O_{ij} \frac{x_i - x_j - (x_i^n - x_j^n)}{\Delta t}\delta_{x_i},$$

since O is symmetric. Now, if we take the time step $\Delta t \to 0$, we acquire

$$\xi \sum_{i=1}^{N} \frac{\mathrm{d}x_i}{\mathrm{d}t}\delta_{x_i} + \eta \sum_{i=1}^{N}\sum_{j=1}^{N} O_{ij}\left(\frac{\mathrm{d}x_i}{\mathrm{d}t} - \frac{\mathrm{d}x_j}{\mathrm{d}t}\right)\delta_{x_i}, \tag{4}$$

which will become a part of the force balance equations.

At this stage, we can also better describe what each term represents physically. For the first term in Equation 4, movement of filament i will be inhibited by the viscosity of the cell's cytoplasm. This corresponds to a frictional force

$$\xi \frac{\mathrm{d}x_i}{\mathrm{d}t},$$

where the ith filament's velocity is slowed depending on drag friction, ξ.

Moving onto the second term in Equation 4, for simplicity, we have let all filaments have the same length l, and assume they are mechanically connected by cross-linking proteins, to avoid bundle disintegration [22]. We represent this in our model as friction between overlapping filaments, since cross-linkers can attach and remain anywhere on a filament until they detach [3]. We achieve this by making cross-linkers the viscous component of the viscoelastic coupling between the proteins and filaments. The friction experienced by filament i due to being connected to another filament j via a cross-linking protein depends on the degree to which they overlap and their relative velocity,

$$\eta O_{ij}\left(\frac{\mathrm{d}x_i}{\mathrm{d}t}-\frac{\mathrm{d}x_j}{\mathrm{d}t}\right),$$

i.e. the closer two filaments are, the more tension is dissipated. We let η be the effective viscous drag due to these cross-linkers. Lastly, we must account for all filaments overlapping filament i by summing these forces and obtain,

$$\eta\sum_{j=1}^{N}O_{ij}\left(\frac{\mathrm{d}x_i}{\mathrm{d}t}-\frac{\mathrm{d}x_j}{\mathrm{d}t}\right).$$

3.2 Myosin Motors

Next, we would like to introduce the component E_m related to the influence of myosin motors to the energy functional (Equation 2). We assume motor k is either connected to two filaments, or none at all. As such, we construct an indicator matrix $\Theta\in\mathbb{M}^{M\times N}$ such that

$$\Theta_{ik}=\begin{cases}1, & \text{if filament } i \text{ is connected to motor } k\\ 0, & \text{else}\end{cases}$$

and

$$\sum_{i=1}^{N}\Theta_{ik}=0 \text{ or } 2,\ \forall\ k=1,\dots,M.$$

This gives us

$$E_m[\mathbf{x},\mathbf{y}]=\sum_{i=1}^{N}\sum_{k=1}^{M}\Theta_{ik}\left(-F_s(x_i-y_k)P_i+\frac{F_s}{V_m}\frac{\left(x_i-y_k-(x_i^n-y_k^n)\right)^2}{2\Delta t}\right) \tag{5}$$

which we describe in this section.

As before, we compute its variation,

$$\begin{aligned}\delta E_m[\mathbf{x},\mathbf{y}]&=\sum_{i=1}^{N}\sum_{k=1}^{M}\Theta_{ik}\left(-F_sP_i(\delta_{x_i}-\delta_{y_k})+\frac{F_s}{V_m}\frac{x_i-y_k-(x_i^n-y_k^n)}{\Delta t}(\delta_{x_i}-\delta_{y_k})\right)\\&=\sum_{i=1}^{N}\sum_{k=1}^{M}\Theta_{ik}\left(-F_sP_i+\frac{F_s}{V_m}\frac{x_i-y_k-(x_i^n-y_k^n)}{\Delta t}\right)(\delta_{x_i}-\delta_{y_k}).\end{aligned}$$

After taking $\Delta t\to 0$, we obtain

$$\sum_{i=1}^{N}\sum_{k=1}^{M}\Theta_{ik}\left(-F_sP_i+\frac{F_s}{V_m}\left(\frac{\mathrm{d}x_i}{\mathrm{d}t}-\frac{\mathrm{d}y_k}{\mathrm{d}t}\right)\right)(\delta_{x_i}-\delta_{y_k}), \tag{6}$$

which will also make up part of our force balance equations. As for the physical interpretation of these terms, the δ_{y_k} terms (i.e. the perspectives of each motor k) describe an affine force-velocity relationship,

$$F(V) = F_s \left(P - \frac{V}{V_m} \right),$$

where F is the force exerted by the motor, V is the relative velocity between the motor and its attached filaments, F_s is the stall motor force, and V_m is the maximum velocity a motor can travel. As presented in Figure 7, the polarity $P^{\pm} = \pm 1$ of the filament directs whether the motor exerts a force to the left ($F < 0$) or right ($F > 0$), since the motor is attracted to the plus ends of the connected filaments.

Similarly, the force as experienced by the connected filament i acts in the opposite direction. This is why the sign of the δ_{x_i} terms is switched in the final force balance equations (Section 3.4).

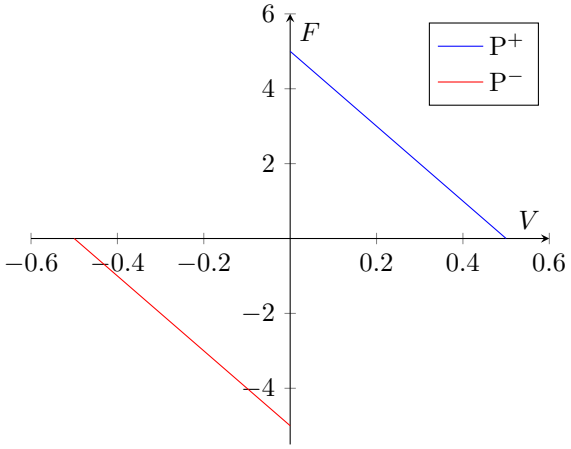

Figure 7: Force-Velocity Relationship of Myosin Motors

3.3 Focal Adhesions

Lastly, we need to construct the mechanism which describes the cell's points of contact with the extracellular matrix, the focal adhesions. This makes up the final component of the energy functional (Equation 2),

$$E_a[\mathbf{x}, \mathbf{z}] = \frac{k}{2} \left(z_B - z_A - L \right)^2 + \rho \sum_{i=1}^{N} \sum_{j=A,B} O_{ij}^a \frac{\left(x_i - z_j - (x_i^n - z_j^n) \right)^2}{2\Delta t}, \tag{7}$$

where $L = z_B^1 - z_A^1$ is the equilibrium length of the stress fibre. Once again, we compute the variation

$$\begin{aligned} \delta E_a[\mathbf{x}, \mathbf{z}] = {} & k \left(z_B - z_A - L \right) \left(\delta_{z_B} - \delta_{z_A} \right) \\ & + \rho \sum_{i=1}^{N} \sum_{j=A,B} O_{ij}^a \frac{x_i - z_j - (x_i^n - z_j^n)}{\Delta t} (\delta_{x_i} - \delta_{z_j}) \end{aligned}$$

and take $\Delta t \to 0$ to obtain

$$k \left(z_B - z_A - L \right) \left(\delta_{z_B} - \delta_{z_A} \right) + \rho \sum_{i=1}^{N} \sum_{j=A,B} O_{ij}^a \left(\frac{\mathrm{d}x_i}{\mathrm{d}t} - \frac{\mathrm{d}z_j}{\mathrm{d}t} \right) (\delta_{x_i} - \delta_{z_j}). \tag{8}$$

The first term has this structure because we aim to measure the contractile force the stress fibre generates in order to pull the cell along. As such, we define the two end points, $\mathbf{z} = (z_A, z_B)$, and model this interval as a stiff spring ($k \gg 0$). Preferably, the model would be constrained such that the focal adhesions were fixed in position, however penalising large deviations from this equilibrium length relaxes this constraint allowing for end points to move slightly so that the force can be measured more readily.

Then, for the second term, we need to ensure these points are connected to the structure. We achieve this by making the end points the centre of adhesion areas of length $\bar{l} < l$ and introducing another friction term, similar to that created for cross-linker proteins, which prevents filaments overlapping the focal adhesions from disconnecting easily. Drag friction $\rho \gg 0$ ensures the relative velocity between filaments overlapping the end points are essentially zero, and each element of $O^a \in \mathbb{M}^{N\times 2}$ describes the overlap between a filament and the focal adhesion.

Therefore, we have reached the final component of our original energy functional (Equation 2).

3.4 Force Balance Equations

So far, we have determined the variation of the original energy functional (Equation 2). By combining the results (Equations 4, 6 and 8), we obtain the total variation

$$\begin{aligned}\delta E =& \xi \sum_{i=1}^{N} \frac{\mathrm{d}x_i}{\mathrm{d}t}\delta_{x_i} + \eta \sum_{i=1}^{N}\sum_{j=1}^{N} O_{ij}\left(\frac{\mathrm{d}x_i}{\mathrm{d}t} - \frac{\mathrm{d}x_j}{\mathrm{d}t}\right)\delta_{x_i} \\ &+ \sum_{i=1}^{N}\sum_{k=1}^{M} \Theta_{ik}\left(-F_s P_i + \frac{F_s}{V_m}\left(\frac{\mathrm{d}x_i}{\mathrm{d}t} - \frac{\mathrm{d}y_k}{\mathrm{d}t}\right)\right)(\delta_{x_i} - \delta_{y_k}) \\ &+ k\,(z_B - z_A - L)\,(\delta_{z_B} - \delta_{z_A}) \\ &+ \rho \sum_{i=1}^{N}\sum_{j=A,B} O^a_{ij}\left(\frac{\mathrm{d}x_i}{\mathrm{d}t} - \frac{\mathrm{d}z_j}{\mathrm{d}t}\right)(\delta_{x_i} - \delta_{z_j}) = 0,\end{aligned}$$

which we set to zero to determine where extremal values occur. Since all admissable variations $\delta_{x_i}, \delta_{y_k}, \ldots$ are arbitrary, their coefficients must all equal zero and we obtain the system of equations

$$\begin{cases} \xi\dfrac{\mathrm{d}x_i}{\mathrm{d}t} + \eta\displaystyle\sum_{j=1}^{N} O_{ij}\left(\frac{\mathrm{d}x_i}{\mathrm{d}t} - \frac{\mathrm{d}x_j}{\mathrm{d}t}\right) + \sum_{k=1}^{M}\Theta_{ik}\left(-F_s P_i + \frac{F_s}{V_m}\left(\frac{\mathrm{d}x_i}{\mathrm{d}t} - \frac{\mathrm{d}y_k}{\mathrm{d}t}\right)\right) \\ \qquad +\rho\displaystyle\sum_{j=A,B} O^a_{ij}\left(\frac{\mathrm{d}x_i}{\mathrm{d}t} - \frac{\mathrm{d}z_j}{\mathrm{d}t}\right) = 0, \text{ for } i = 1,\ldots,N \\ \displaystyle\sum_{i=1}^{N}\Theta_{ik}\left(F_s P_i - \frac{F_s}{V_m}\left(\frac{\mathrm{d}x_i}{\mathrm{d}t} - \frac{\mathrm{d}y_k}{\mathrm{d}t}\right)\right) = 0, \text{ for } k = 1,\ldots,M \\ k\,(z_B - z_A - L) - \rho\displaystyle\sum_{i=1}^{N} O^a_{iB}\left(\frac{\mathrm{d}x_i}{\mathrm{d}t} - \frac{\mathrm{d}z_B}{\mathrm{d}t}\right) = 0 \\ k\,(z_B - z_A - L) + \rho\displaystyle\sum_{i=1}^{N} O^a_{iA}\left(\frac{\mathrm{d}x_i}{\mathrm{d}t} - \frac{\mathrm{d}z_A}{\mathrm{d}t}\right) = 0 \end{cases}$$

as our force balance equations for each filament i, motor j and end point respectively. This makes sense if we relate them to Newton's second law of motion. Since masses are small, inertial forces are negligible as compared to these frictional forces. As a result, the sum of all frictional forces acting on each component should equal zero.

For completeness, these equations were derived from the energy functional

$$
\begin{aligned}
E[\mathbf{x},\mathbf{y},\mathbf{z}] = \xi \sum_{i=1}^{N} \frac{(x_i - x_i^n)^2}{2\Delta t} + \eta \sum_{i=1}^{N}\sum_{j=1}^{N} \frac{O_{ij}}{2} \frac{\left(x_i - x_j - (x_i^n - x_j^n)\right)^2}{2\Delta t} \\
+ \sum_{i=1}^{N}\sum_{k=1}^{M} \Theta_{ik} \left(-F_s(x_i - y_k)P_i + \frac{F_s}{V_m} \frac{\left(x_i - y_k - (x_i^n - y_k^n)\right)^2}{2\Delta t} \right) \\
+ \frac{k}{2}\left(z_B - z_A - L\right)^2 + \rho \sum_{i=1}^{N} \sum_{j=A,B} O_{ij}^a \frac{\left(x_i - z_j - (x_i^n - z_j^n)\right)^2}{2\Delta t}
\end{aligned}
$$

which was described in Equation 2 and defined by Equations 3, 5 and 7.

4 Numerical Scheme

The steepest descent scheme (Equation 1) was also used as a numerical scheme, which was implemented in the programming language Julia using the `Optim.jl` package for energy minimisation. All code can be found on Github [6].

4.1 Toy Model

We introduce a simple configuration of the model, which has a single motor connected to two filaments with opposing polarity, to demonstrate the model functioning. We refer to this setup as the toy model, as depicted in Figure 8, and describe how it behaves in the simulation in Figure 9. Essentially, the motor exerts a force that causes the stress fibre to contract, but later causes the stress fibre to expand.

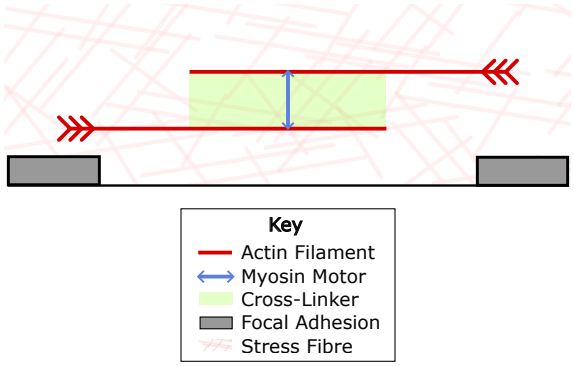

Figure 8: One dimensional interpretation of the toy model.

If we randomise the starting position of filaments in this toy model, it can result in both a contractile (negative) or expansive (positive) force. In Figure 10, each line corresponds to a different, random, initial stress fibre configuration, with y_o describing the initial position of the motor relative to the filament's plus end. $y_o < 0.5$ describes when the motor is initially closer to the minus end of the filaments, whereas when $y_o > 0.5$ it is initially closer to the plus ends. As demonstrated by the area under these contractile force curves, expansive forces are more common. This is because the single motor structures have a tendency to expand once the motor is close to both plus ends of the filaments. More specifically, if the motor starts close to the minus end of a filament, it causes the filaments to attract until the motor passes the centre of a filament which, since the plus ends

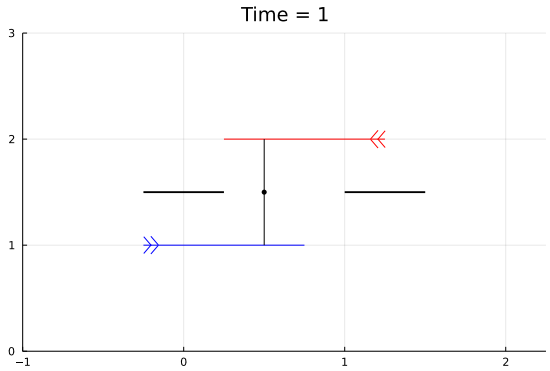

(a) Initially, the stress fibre starts with the motor connected closer to its filaments' minus ends.

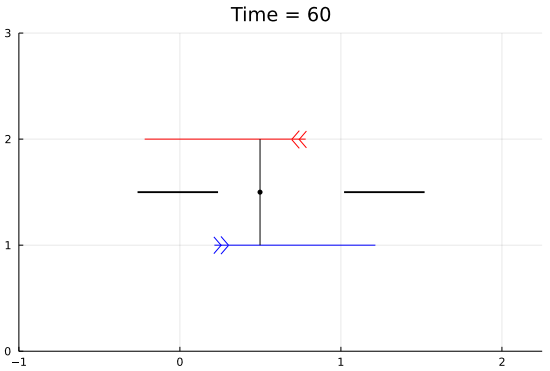

(b) The filaments now heavily overlap, which maximises cross-linking drag and slows motor movement until the motor is closer to the plus ends of the filaments.

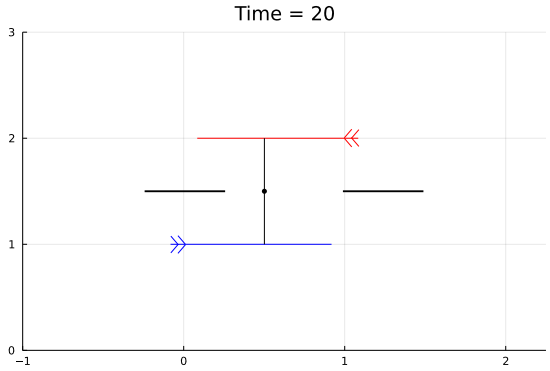

(c) Next, the opposing polarities of the filaments causes the focal adhesions to come together slightly, and the stress fibre contracts.

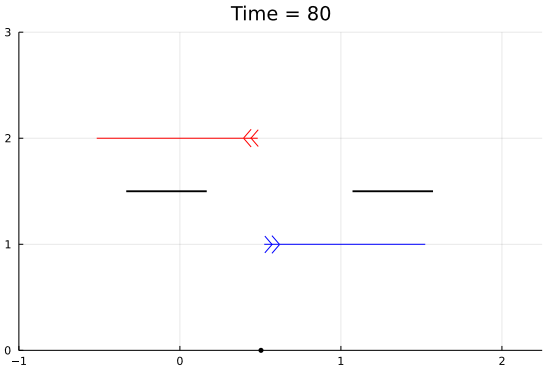

(d) Focal adhesions are pushed apart, meaning the stress fibre expands, until the motor reaches the end of a filament and detaches. The detached motor sits at the bottom of the simulation, and the stress fibre returns to its equilibrium position.

Figure 9: Snapshots of toy model over time (read top-bottom, left-right), with $N = 2$, $M = 1$, $l = 1$, $L = 1.25$. Horizontal axis is position in space, whereas the vertical axis uniquely labels each filament. The thick black intervals signify focal adhesions and the vertical black line represents a connection between the motor (black dot) and its attached filaments. The barbs on the filaments indicate filament plus ends, and so red filaments are oriented with the plus end on the right, and blue filaments have their plus end on the left. These barbs are omitted in future for simplicity.

are being pulled together, pushes the overlapping filaments apart. Similarly, if the motor initially attaches closer to the plus end, the filaments will still be pushed apart. This is before it reaches a peak expansive force and abruptly goes to zero. This behaviour corresponds to when the motor detaches, and so there is no force keeping the stress fibre stretched. Due to its elastic behaviour, the stress fibre returns to its equilibrium length. Thus, the single motor structure has a tendency to expand, and we needed to explore mechanisms that could reduce it. Section 4.2 describes one such mechanism.

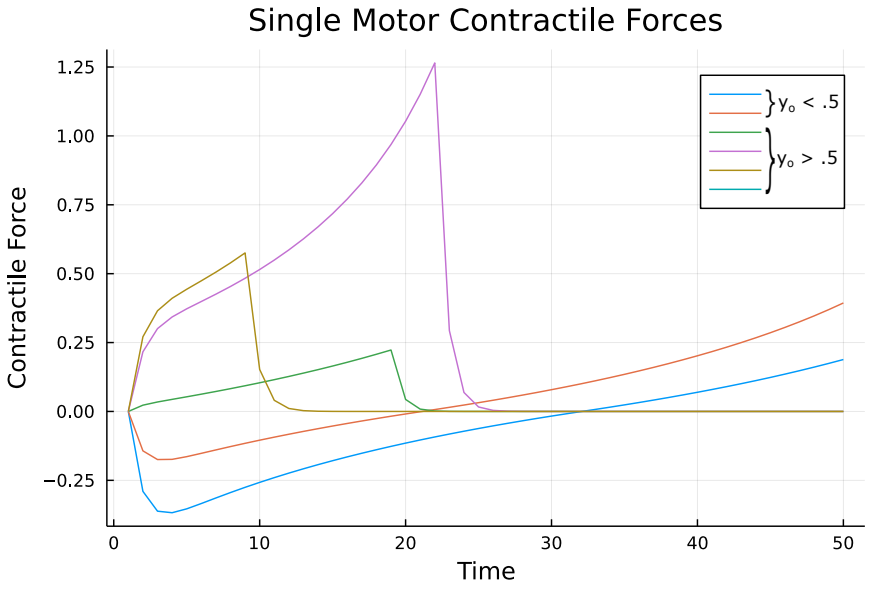

Figure 10: Contractile force of single motor attached to two filaments of opposing polarity.

Whilst it is unlikely for a motor to randomly connect at the minus end of both its attached filaments, we now introduce a symmetric toy model (see Figure 11) to demonstrate how it is possible for the model to exhibit equally contractile and expansive motions as well as validate model implementation. Since the configuration is symmetric, any force generated has an equivalent force acting in the opposite direction, and the motor remains in the same position. We also make the stress fibre extremely stiff to ensure the friction between filaments and the focal adhesions remain consistent. This prohibits the focal adhesions from moving much, however it keeps the overlap between the filaments and focal adhesion roughly the same, allowing us to analytically derive an equation to measure the stress imposed on the system.

As seen in Figure 12a, starting the motor at the minus ends of the filaments means that the stress fibre experiences a contractile force equivalent to the expansive force. So, in this particular scenario, it would be unnecessary to remove the expansive bias. However, motors can attach at any point along a filament, and hence it is unlikely for the stress fibre to randomly be configured in this way. Additionally, the figure highlights the model's nonlinear behaviour, which is necessary in a rigid filament model according to Lenz et al. (2012) [15]. We first remark that the rate at which contraction decreases slows as the motor approaches the centre of the filaments. Then, the rate of expansion increases as the motor approaches the filaments' plus ends.

The original toy model (Figure 14) also exhibits this behaviour, and it occurs because of how we have modelled cross-linking proteins. We have abstracted the effect of cross-linkers as simply friction between overlapping filaments. As a result, when filaments have a greater overlapping length, such as when the motor is at their centre, they experience a greater resistant force. So, when filaments are

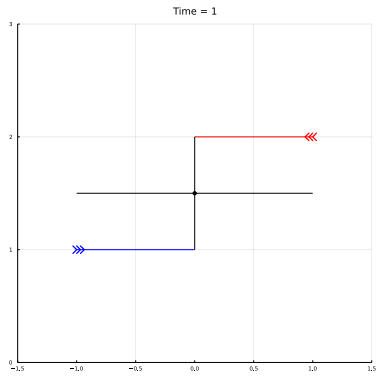

(a) The stress fibre's single motor is connected to the filaments' minus ends.

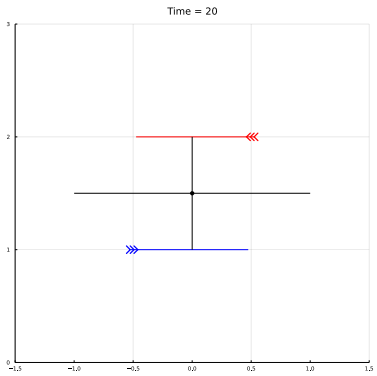

(b) Motion slows at maximum overlap of filaments, due to cross-linkers.

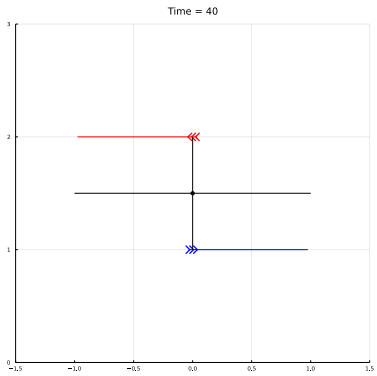

(c) With little friction, the motor quickly reaches the filaments' plus ends.

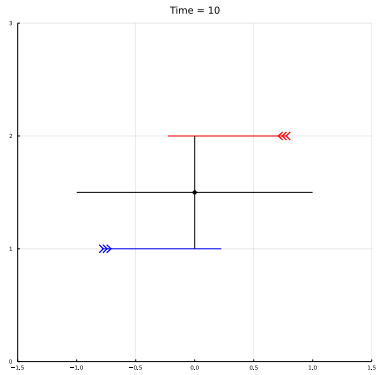

(d) Attracted to their plus ends, the motor pulls the filaments together.

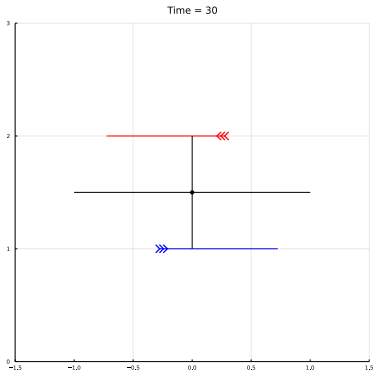

(e) Closer to their plus ends, the motor starts to push the filaments apart.

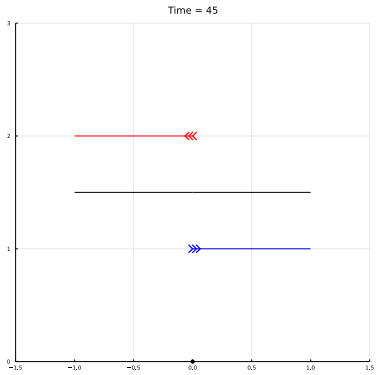

(f) The motor detaches.

Figure 11: Snapshots of symmetric toy model over time (read top-bottom, left-right), with $k = 1000$, $N = 2$, $M = 1$, $l = 1$, $L = 1.25$, $\bar{l} = 1$. Horizontal axis is position in space, whereas the vertical axis uniquely labels each filament. The thick black intervals signify focal adhesions and the vertical black line represents a connection between the motor (black dot) and its attached filaments. The barbs on the filaments indicate filament plus ends, and so red filaments are oriented with the plus end on the right, and blue filaments have their plus end on the left.

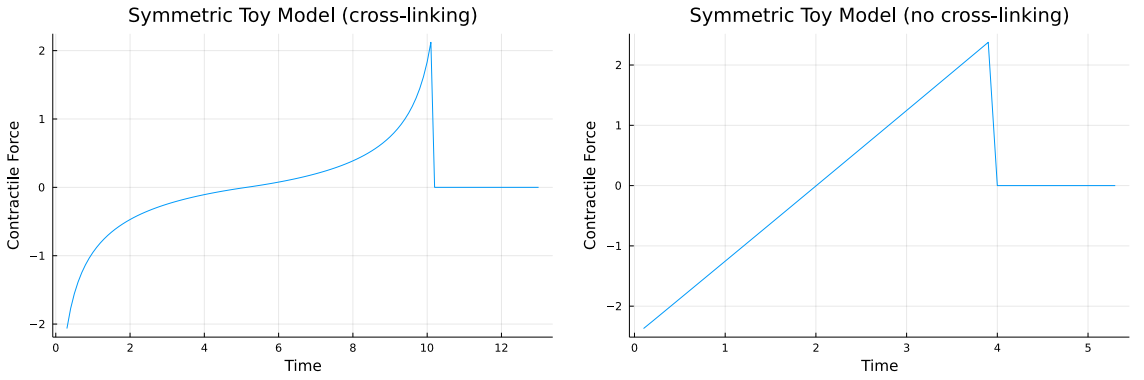

(a) Symmetric toy model with cross-linking proteins. **(b)** Symmetric toy model without cross-linking proteins.

Figure 12: Contractile force of symmetric toy model, where a single motor starts attached to the minus end of two opposing filaments.

pushed apart by the motor, their overlap is reduced, friction is mitigated, and the rate of expansion increases. This is supported by Figure 12b because, after removing cross-linking proteins ($\eta = 0$), the contractile force increases linearly over time.

The symmetric toy model configuration additionally allows us to construct the following expression for the stress experienced by the symmetric toy model stress fibre,

$$\sigma(t) = \frac{2\rho F_s}{(\xi + \frac{F_s}{V_m} + \rho l)^2} t - \frac{\rho F_s}{\xi + \frac{F_s}{V_m} + \rho l}.$$

Full derivation can be found in the supplementary material (Section 8.1). As we can see in Figure 13, this function accurately describes the contractile force measured in our simulations until the motor detaches. This serves as a validation that the numerical scheme has been correctly implemented.

4.2 Fast-Sliding Motors

Tam, Mogilner and Oelz (2022) found that, on semi-flexible filaments, motors tend to slide off the filaments quickly as they approach their plus ends, and this facilitated contraction [21]. In the coming investigation of the toy model, we propose an equivalent fast motor slide-off mechanism in 1D to improve stress fibre contractility.

In Figure 14, we found the contractile force of the toy model whilst varying the point along the filaments at which the motor detaches. We defined this drop-off point δ as the distance from the filament's plus end, i.e. $\delta = 0$ for the case where the motor drops off precisely at the plus end of the filament. When the motor drops-off before the plus end ($\delta > 0$), we call this an early motor drop-off.

As demonstrated by the area under the blue curve (in Figure 14), the motor detaching at the plus end of the filament suggests the stress fibre favours an expansive motion, as before. However, as the motor detaches further and further away from the plus end (δ increases), the area beneath the curve becomes more balanced between positive and negative, and so the stress fibre starts to spend an equal amount of time expanding and contracting, thus removing the bias towards expansion. Furthermore, when the motor drop-off point is in or before the centre of the filament, the stress fibre only contracts because the motor detaches before the stress fibre has a chance to expand. These results support the conclusion found in *F-Actin Bending Facilitates Net Actomyosin Contraction By*

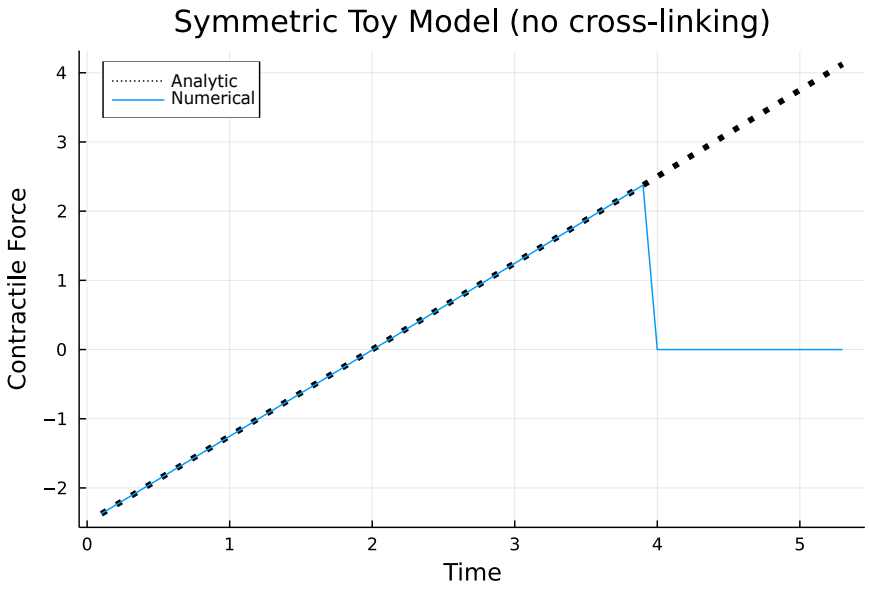

Figure 13: Contractile force of symmetric toy model, with analytic solution overlaid.

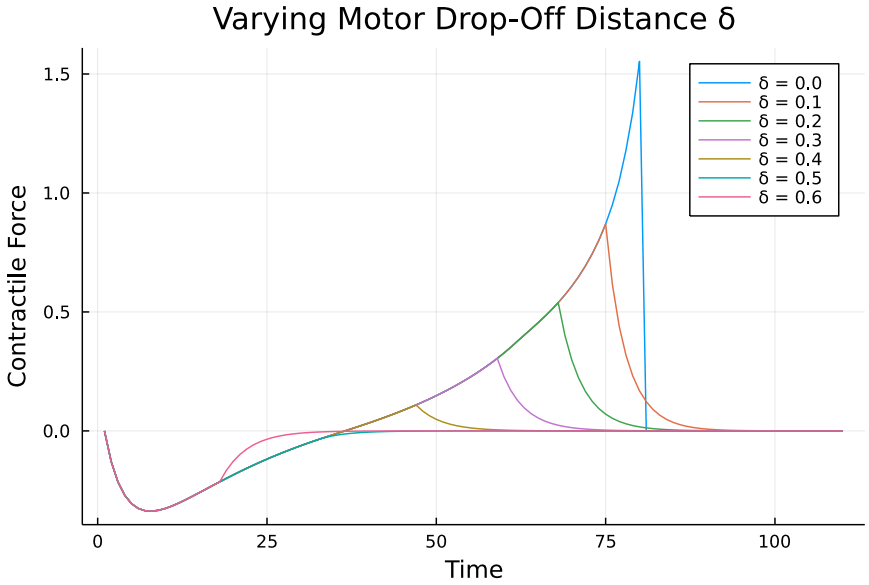

Figure 14: Contractile force of a single motor attached to two filaments of opposing polarity, with the motor detaching at various distances from the plus end of the filaments.

Inhibiting Expansion With Plus-End-Located Myosin Motors [21], and hence prompted the computational study into whether early motor drop-offs could facilitate contraction in more complicated stress fibre structures (Section 5).

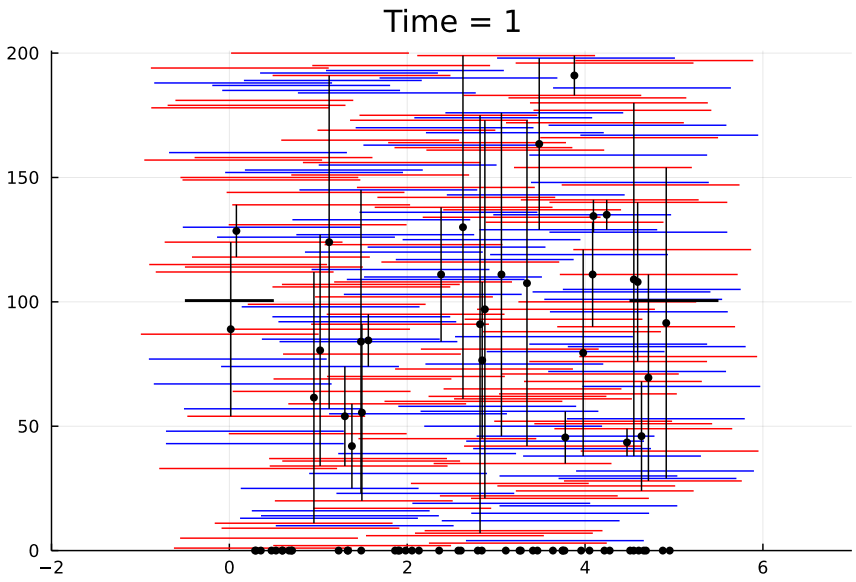

Figure 15: Simulation of complex stress fibre structure ($N = 200$, $M = 75$, and $L = 5$).

4.3 Reference Model

The model can solve for large N and M (see Figure 15), with execution times varying depending on how long the stress fibre is evolved for and whether it is chosen to visualise the simulation. There is an upper limit to the number of degrees of freedom the model can handle however. If it is too high, then the scheme does not converge to a minimum. This is usually visually clear, with the motors sporadically detaching and reattaching with little to no filament movement. As a result, in order to scale the model to study more complex stress fibre structures, we needed to find an appropriate balance between parameters. More specifically:

- filaments had to be long enough to encourage motor attachment,
- the stress fibre had to be long enough to prevent excessive friction between heavily overlapping filaments,
- the number of filaments had to be great enough to fill the length of the stress fibre and prevent breaking, and
- the number of motors had to be great enough to facilitate motion.

All of this had to be achieved whilst minimising computational complexity, since the upper limit of degrees of freedom in the model has not been determined. The exploration into identifying the appropriate balance of these parameters is described in the supplementary material (Section 8.2).

Table 1 summarises the parameter values relating to the simulation, whereas Table 2 states the parameters that relate to the physical aspects of the model. We refer to these parameters as the reference parameters, and they are the default parameters we use to perform our investigation (unless otherwise stated).

4.4 Pattern Formations

With the model as it has been described, several issues arose that caused unfavourable and physically inaccurate scenarios. This section describes these issues, and the methods that were introduced to

Description	Symbol	Value
Drag friction on actin filaments	ξ	0.0000001 pN s µm^{-2}
Drag friction on edge actin filaments	ρ	10 pN s µm^{-2}
Spring constant of stress fibre	k	10 pN µm^{-1}
Length of focal adhesions	$\bar{l}$	1 µm
Time step	Δt	0.1 s
Number of time steps	T	250

Table 1: List of reference parameters chosen for the numerical scheme. Parameter ξ was chosen to be arbitrarily small to ensure computational stability. Similarly, ρ, k are arbitrarily large to emphasise the (relaxed) constraint that focal adhesions are fixed. Lastly, time was chosen such that late-time stress fibre behaviours would still be observed.

Description	Symbol	Value
Equilibrium length of stress fibre	L	8 µm
Length of actin filaments	l	2 µm
Number of actin filaments	N	20
Number of myosin motors	M	10
Stall force for myosin motors	F_s	5 pN
Load-free myosin velocity	V_m	0.5 µm s^{-1}
Effective viscous drag due to cross-linkers	η	15 pN s µm^{-2}
Motor drop-off distance	δ	0 µm
Rate of filament turnover	α	0 s^{-1}
Rate of motor turnover	β	0 s^{-1}

Table 2: List of physical reference parameters. The lengths were chosen as described in the supplementary material 8.2. Parameters F_s, V_m were sourced from literature [19], and the remaining are introduced (and changed) in Section 5, as a result of our investigation.

the model to mitigate their effect.

Polarity sorting (see Figure 16), is where the filaments with the same orientation end up at one end of the stress fibre and those opposing at the other. If time progresses for long enough and there is enough overlap between filaments, stress fibres usually evolve into this state. It is where all plus ends of filaments migrate to the centre of the stress fibre, with the motors having pushed the filaments apart. A stress fibre in this state cannot extend nor contract because there is no overlap between opposing filaments for motors to attach and undo the sorting. As such, it was a scenario we hoped to mitigate in the model.

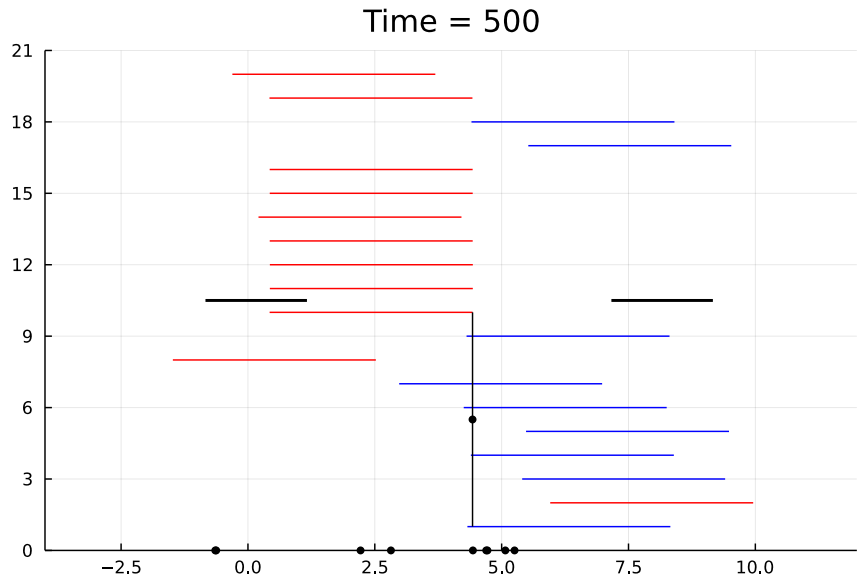

Figure 16: End of simulation ($\eta = 0.01$, $L = 4$) to illustrate polarity sorting, where filaments of the same polarity are grouped at opposing ends of the stress fibre.

The initial configuration of the stress fibre seemed to be the main cause of this occurring, however we wanted to keep the initial positions of filaments and motors randomised. Like Hiraiwa et al. (2016), we decided to introduce filament turnover (see Figure 17). We introduced a probability α of a filament's position being randomised in a time step.

We can visualise filament turnover in the simulation if we track the position of a subset of filaments over time. In Figure 18a, we see the original evolution of eight filaments in a stress fibre, and in Figure 18b, we have the same eight filaments but now responding to filament turnover. The horizontal jumps correspond to a turnover event. Although α needs to be chosen such that the stress fibre maintains tension whilst still fulfilling its purpose, it does not increase the complexity of our one-dimensional model, which made it the most acceptable candidate. Further study will be required to determine how effectively filament turnover discourages polarity sorting, however it appeared to improve contractility, and hence became a part of our investigation.

Another unfavourable configuration was when a motor was permanently inactive (see Figure 19a). When a stress fibre started with, or evolved such that, a motor overlapped less than two filaments, the motor would remain stationary, preventing that section of stress fibre from moving. Therefore, motor turnover was implemented so that at each time step there was a probability β that a motor had its position randomised. This meant if an inactive motor remained stationary, it was unlikely it would remain stationary. Similar to filament turnover, motor turnover also seemed to improve

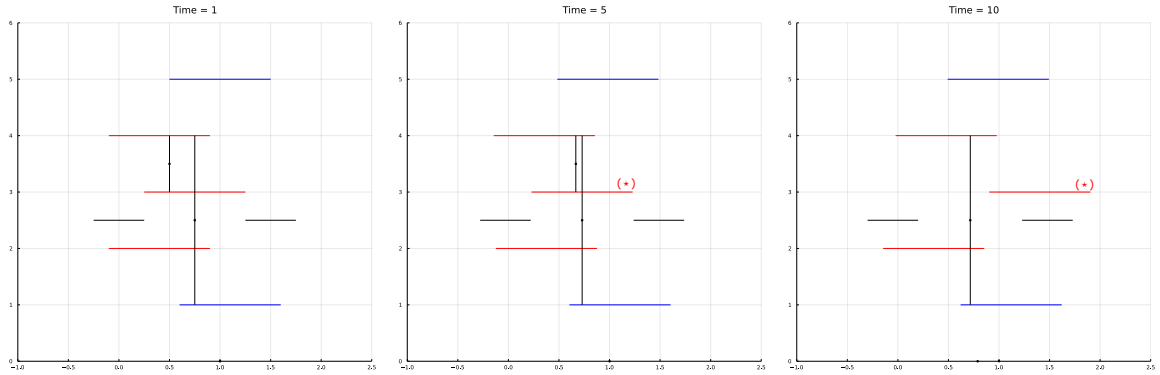

(a) Initial stress fibre configuration that could become polarity sorted.

(b) Stress fibre starts contracting, with actin filament ⋆ labelled.

(c) Actin filament ⋆ turns over, randomising its position.

Figure 17: Demonstrating filament turnover to prevent polarity sorting on simple stress fibre configuration with $N = 5$, $M = 3$, $L = 1.5$, $l = 1$, and $\alpha = 0.05$.

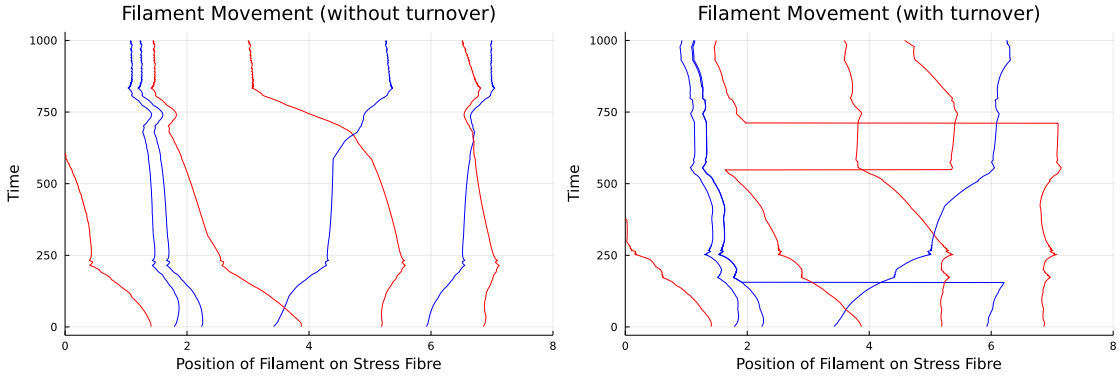

(a) No filament turnover ($\alpha = 0$).

(b) With filament turnover ($\alpha = 0.001$).

Figure 18: Position in reference stress fibre of eight filaments over time. Coloured to match polarity of filament.

contractility, and became a part of our investigation.

As a summary, we needed to prevent (unphysical) behavioural patterns from emerging. We achieved this by introducing a stochastic turnover of filaments and motors, like Hiraiwa et al. (2016) [11]. We believe turnover could encompass physical mechanisms that are missing due to the simplistic nature of the model.

5 Results

Randomising the initial stress fibre configuration can generate both a contractile (negative) or expansive (positive) force for reference simulation parameters. As seen in Figure 20, without early motor detachment ($\delta = 0$), filament turnover ($\alpha = 0$) or motor turnover ($\beta = 0$), the contractile force measured for a reference stress fibre has a less predictable path as compared to the toy model (Figure 10). This is because there are more motors detaching and reattaching to generate forces,

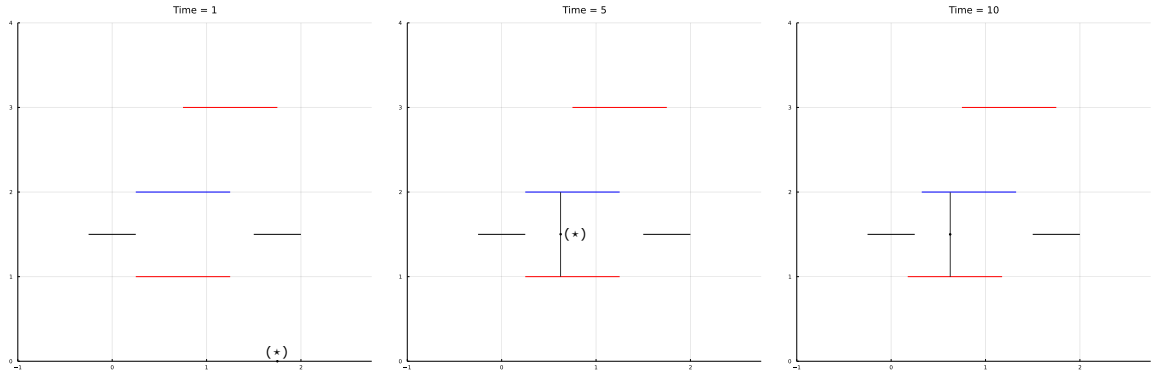

(a) Motor $\star$ inactive due to overlapping only one filament, and stress fibre is stationary as a result.

(b) Motor $\star$ turns over, randomising its position, and attaches to its new neighbouring filaments.

(c) Stress fibre movement restored.

Figure 19: Demonstrating motor turnover as a way to facilitate stress fibre movement on a simple stress fibre configuration with $N = 3$, $M = 1$, $L = 1.75$, $l = 1$, $\alpha = 0$, $\beta = 0.1$.

and there is a greater selection of filaments for them to attach to. However, the model still had a tendency for stress fibres to expand rather than contract, as demonstrated by the area under these curves. As a result, we implemented several mechanisms to remove this bias towards expansion, including early motor drop-offs, filament turnover and motor turnover. In this section, we investigate their ability to induce stress fibre contraction.

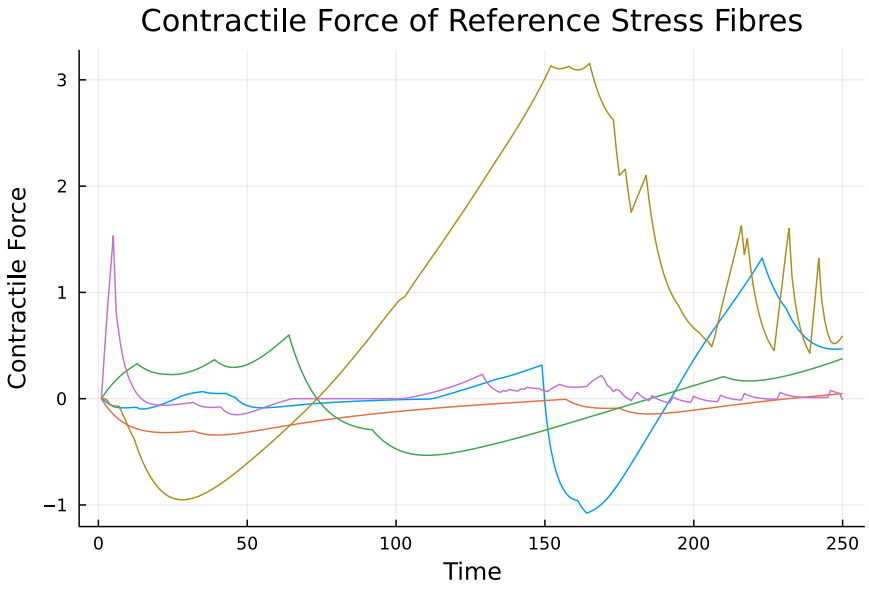

Figure 20: The contractile force of five stress fibres with the same reference parameters given in Table 1. Starting each with a random initial configuration, and evolving with no early motor drop-offs, filament or motor turnover ($\delta = \alpha = \beta = 0$), for $T = 250$ time steps. Positive contractile forces corresponds to expansion, and negative is contraction.

5.1 Early Motor Drop-Offs

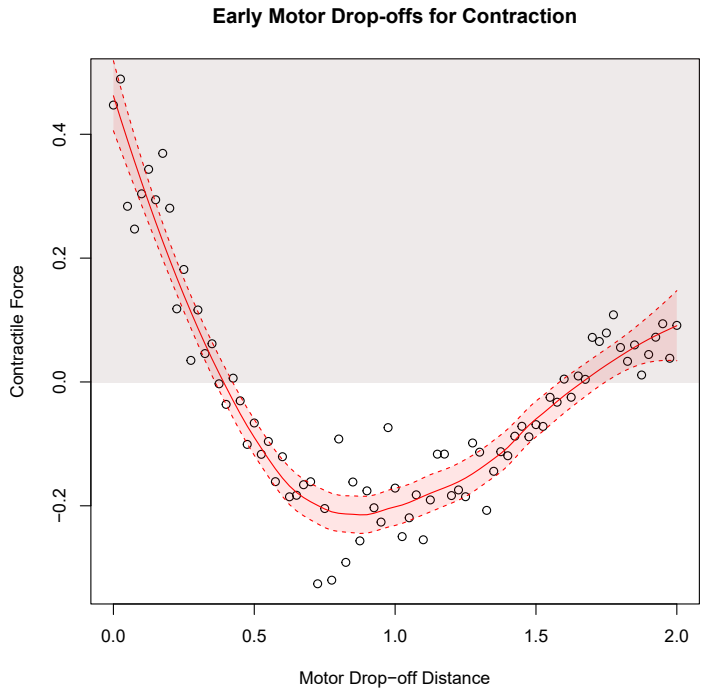

Figure 21: LOESS regression of mean contractile force of 25 reference parameter trials for each motor drop-off distance δ (measured in µm). Region of contraction is highlighted in white.

Using the Julia package `RCall` we were able to utilise the R package `SpatialEco` to perform a LOESS regression, which is a generalisation of a moving average, with 99% confidence intervals overlaid. Figure 21 is the result of one such process, where we visualised the relationship between the motor drop-off distance δ and the contractile force, as measured by the mean contractile force of 25 different reference stress fibres for each point.

Similar to the toy model, we see the stress fibre tends to expand if δ is close to zero (the plus end). This expansive force weakens as the motor drop-off distance increases, until around the centre of the filament ($\delta = 1$) the stress fibre tends to contract. This is because we inhibit locally expansive behaviours between a motor and its attached filaments by disconnecting the motor before expansion occurs. This introduces an asymmetry over the entire stress fibre, allowing contraction to be favoured.

In contrast to the toy model, if we increase δ further such that the motor drop-off point is closer to the minus end ($\delta > 1.5$), the stress fibre exerts an expansive force. This is an artefact of the numerical scheme. Motors are still able to attach after the motor drop-off point, but after one time step passes these motors will detach. So, when δ is increased, most motors will behave like this, attaching and detaching immediately. This causes the expansion bias to return albeit weakly since motors cannot generate much force in a single time step. As a result, δ should be small enough to avoid this error whilst large enough for the stress fibre to enter a contractile regime.

5.2 Turnover

In addition to preventing polarity sorting, filament turnover appeared to have an effect on expansion. If we compare the rate at which filaments randomise their position to the mean contractile force (Figure 22a), increasing turnover reduced the frequency of expansive behaviours. Whilst it did not induce contraction, it removed the bias towards expansion. This is because randomising filament positions keeps the filaments uniformly distributed within the stress fibre. It discourages filaments from being positioned outside the stress fibre's equilibrium length, thus inhibiting expansion. On the other hand, if filaments turn over too quickly it does not leave much time for motors to attach and generate a force. As such, filament turnover could improve the model's contractility, but further study is required to determine when filament turnover would prevent movement.

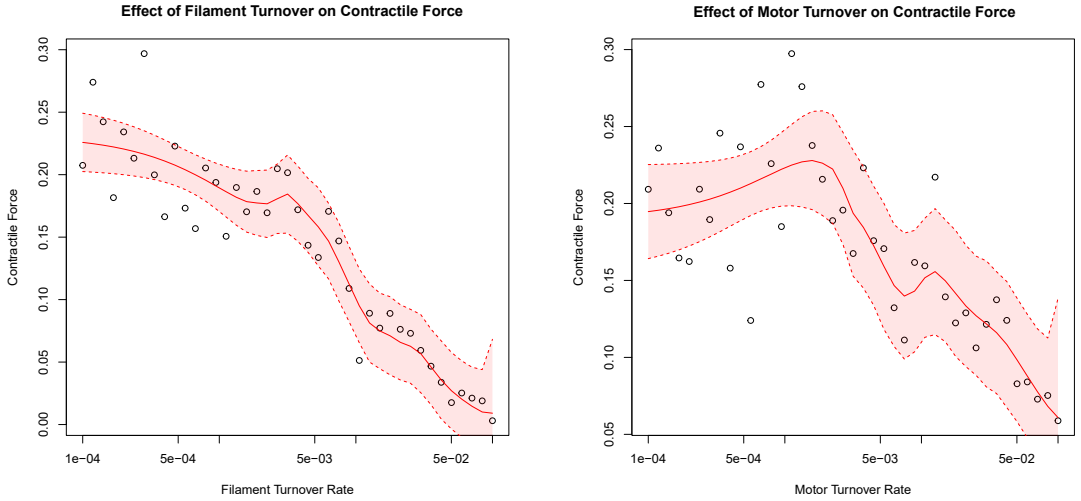

(a) Filament turnover α as a mean of preventing expansive behaviours, where α is the rate of actin filaments randomising their position

(b) Motor turnover β as a mean of preventing expansive behaviours, where β is the rate of myosin motors randomising their position

Figure 22: LOESS Regressions of mean contractile force of 25 reference parameter trials.

Similarly, as well as preventing motor inactivity, motor turnover had an effect on stress fibre contractility. If the time a motor stays attached to a filament reduces, the motor is less likely to exert both an expansive and contractile force. The motor may only stay attached for a period where it attracts its connected filaments, or only repels them. As a result, the expansion bias is reduced. However, motor turnover's effect on contractility is less consistent than filament turnover, with the mean contractile force varying significantly for low values of β. This could suggest that motor turnover is instead preventing movement, since active motors can also turn over and their new position could instead cause them to become inactive. Once again, further study will need to be made to investigate the balance between motor turnover and motor reattachment. Otherwise, investigation into the number of active motors and motor turnover could be worthwhile, to decide whether repositioning only detached motors would improve model contractility.

5.3 Combining Contractile Mechanisms

These LOESS plots (Figures 21, 22) suggest that changing the motor drop-off point to be towards the centre of the filaments could improve a stress fibre's contractility. In contrast, they could indicate that increasing filament and motor turnover could reduce the expansion bias. As such, we visualised

the contractile force of several reference stress fibres with changed parameters, to illustrate their combined effect (see Figure 23). Indeed, making $\delta = 1$, $\alpha = 0.01$, $\beta = 0.01$, appears to have improved stress fibre contractility, with the reference stress fibres generally contracting.

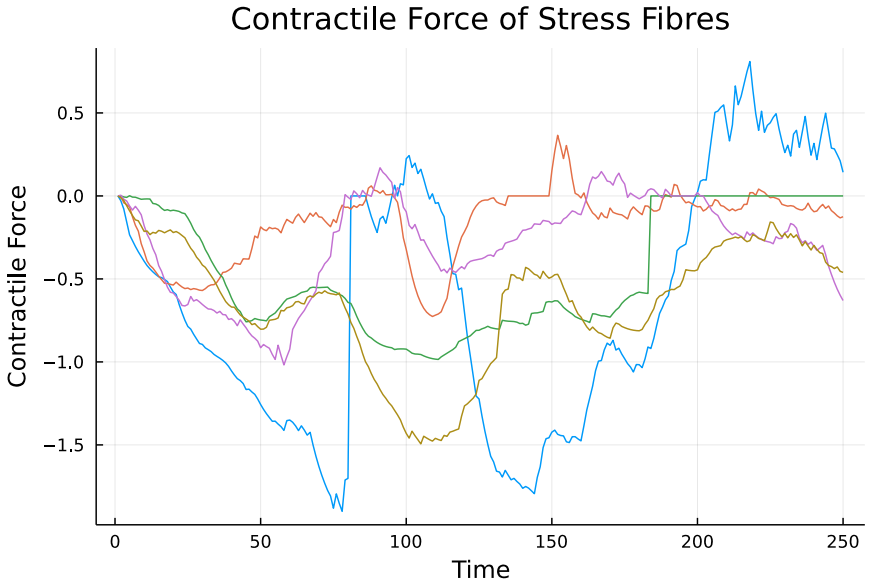

Figure 23: The contractile force of five stress fibres with early motor drop-offs ($\delta = 1$), high filament turnover ($\alpha = 0.01$), and high motor turnover ($\beta = 0.01$), and the reference parameters given in Table 1. Starting each with a random initial configuration, and evolving for $T = 250$ time steps, a positive contractile force corresponds to expansion, and negative is contraction.

The average contractile force of these trials is of a similar magnitude as found in the LOESS plot for δ (Figure 21). We also remark that the LOESS plots for α and β (Figure 22) approach zero as turnover is increased. As such, it is unclear whether filament and motor turnover strengthen contractility by eliminating the bias toward expansion, or whether early motor drop-offs dominate force generation. This motivated a deeper investigation into the relationship between δ, α and β. To explore the combined effects of these variables, we generated the heat maps presented in Figure 24.

Starting with Figure 24a, we vary motor drop-off distances with filament turnover. With motors detaching at the plus end of filaments ($\delta = 0$), we see that increasing filament turnover reduces expansion bias, which reflects what we saw in Figure 22a. As we increase δ however, contraction is induced, with the strongest contractile force occurring when motors drop-off toward the centre of the stress fibre ($\delta = 1$). Once again, this reflects the corresponding LOESS plot (Figure 21), however the magnitude of the maximum contractile force is greater. Introducing filament turnover indeed strengthens the contractile force, however there is no clear trend between increasing filament turnover and this increased strength. This indicates that any amount of filament turnover can promote contraction, as long as it occurs and the motor drop-off distance is within a contractile region.

Then, in Figure 24b, we compare the motor drop-off distance with motor turnover. When motors drop-off toward the centre of filaments, the contraction stress fibres experience is generally stronger than stress fibres with filament turnover. This also means that the motor drop-off region corresponding to contraction is wider than that in the filament turnover case. Moreover, introducing motor turnover weakens the expansive force associated with $\delta = 0$, however increasing β does not

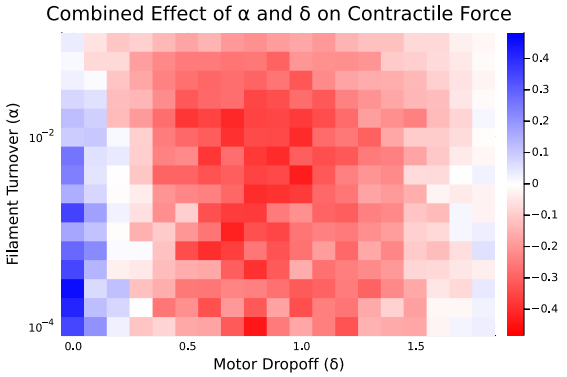

(a) Contractile behaviour in response to different rates of filament turnover α and motor drop-off distances δ. No motor turnover.

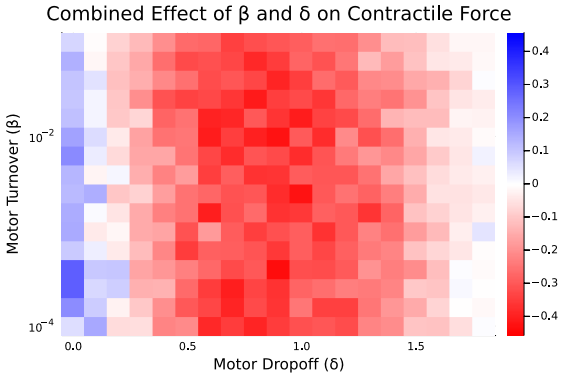

(b) Contractile behaviour in response to different rates of motor turnover β and motor drop-off distances δ. No filament turnover.

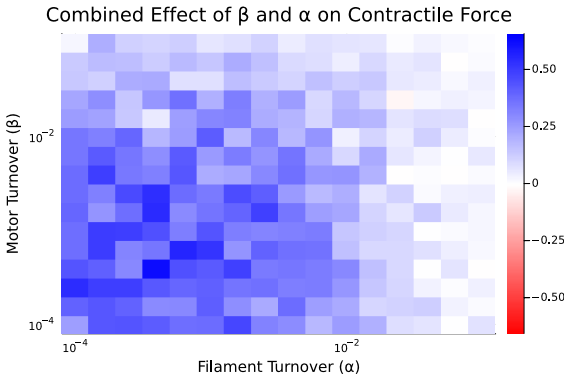

(c) Contractile behaviour in response to different rates of filament turnover α and motor turnover β. No early motor drop-offs.

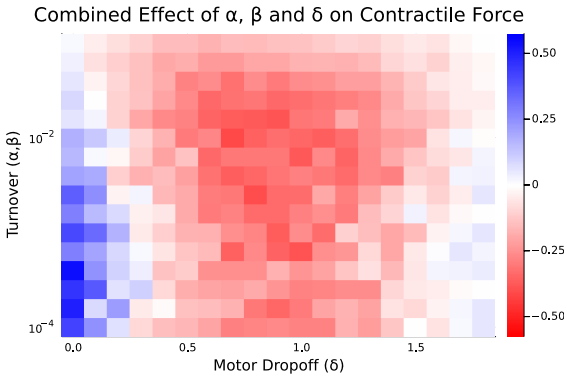

(d) Contractile behaviour in response to motor distances δ and the same rate of turnover α and β.

Figure 24: Average contractile force of reference stress fibres whilst varying turnover and motor drop-offs. Red indicates a contractile force, whereas blue is expansive. Each pixel represents the mean contractile force of 25 stress fibres evolved for 250 time steps.

reduce the expansion bias as much as filament turnover (as in Figure 22b). So, whilst motor turnover performs worse than filament turnover at removing expansion bias, it actually promotes stronger contraction when our motor drop-off distance is within the contractile region.

In Figure 24c, we compare the effect of varying filament and motor turnover. We see that no combinations induced contraction in the structure, suggesting that early motor drop-offs are sufficient for contraction. We also see once again that both forms of turnover either remove the expansion bias so stress fibres are equally likely to expand or contract, or that they inhibit a force to be generated entirely. Either way, turnover does not induce contraction.

Lastly, in Figure 24d we increase both motor and filament turnover and compare it to early motor drop-offs. Whilst introducing turnover previously strengthened contraction, introducing both forms of turnover at once results in the same maximum strength of contraction as if we had introduced no turnover at all. This suggests that introducing both forms of turnover at once becomes too much, and prevents motors from attaching and generating a force. Alternatively, the two forms of turnover could be working against each other, since there would now be double the chance for filaments and their attached filaments from randomly being disconnected, thus reducing the strength of stress fibre contraction. Overall, we realise that introducing both forms of turnover is unnecessary to induce contraction.

6 Discussion

Thus, early motor drop-offs are sufficient for our minimal model stress fibres to favour contraction. This result supports that 1D early motor drop-offs replicate the 2D fast-motor slide-off necessary to induce contraction in the semi-flexible model proposed in *F-Actin Bending*... [21]. We could also predict that myosin in stress fibres do detach before they reach the plus end of their attached filaments. However, it is unknown how frequently these drop-offs would occur biologically, as well as what would cause motors to detach in this region as opposed to the plus end of the filaments. It also may be difficult to verify because the bundles of actin filaments are dense, making it infeasible to track a single motor relative to the filaments it is attached to. As such, we cannot ascertain how closely early motor drop-offs would reflect reality.

Moreover, whilst increasing turnover removed the expansion bias, increasing it did not strengthen contraction. Any amount of filament or motor turnover exhibited a similar maximum contractile force. However, weaker contractile forces were exhibited when both forms of turnover were present. This reflects the results in *Role of Turnover*... where too much turnover prevented the stress fibre from holding tension [11]. Hence, low amounts of turnover are recommended to maximise the stress fibres' ability to contract. This was emphasised by Hiraiwa et al. when they explained that turnover had to occur over a larger time horizon than motor movement [11]. Low turnover could also better reflect nature, as high turnover would suggest the stress fibres constantly regenerate filaments and their motors constantly seek new filaments to attach to.

7 Further Study

Having established our model, we have obtained a microscopic explanation for a stress fibre's contractile nature, but it is difficult to verify because of the length scale. Therefore, in future simulations, we would like to investigate whether the macroscopic system reacts similarly to the results found in in vitro experiments. One such scenario would be subjecting the stress fibre to laser ablation to determine whether severing the model stress fibre would shrink in the same manner as real-life. This would give us the best opportunity to validate our model.

We could also examine the effect of changing the properties of the actin filaments (e.g. to reflect

chemical changes) on the behaviours of the model stress fibre. For example, we could look into representing the extracellular matrix in which the stress fibres exist. This would allow us to investigate mechanotransduction and how the model stress fibre responds to changes in its external environment.

8 Supporting Material

8.1 Derivation of the Contractile Force of Symmetric Toy Model

Assuming that drag due to cross-linking proteins is nil, our force balance equations for the symmetric toy model (Figure 11) are

$$\begin{cases} \xi\dfrac{\mathrm{d}x_i}{\mathrm{d}t} - F_sP_i + \dfrac{F_s}{V_m}\left(\dfrac{\mathrm{d}x_i}{\mathrm{d}t} - \dfrac{\mathrm{d}y_1}{\mathrm{d}t}\right) + \rho\displaystyle\sum_{j=A,B} O^a_{ij}\left(\dfrac{\mathrm{d}x_i}{\mathrm{d}t} - \dfrac{\mathrm{d}z_j}{\mathrm{d}t}\right) = 0, \text{ for } i = 1,2 \\ \displaystyle\sum_{i=1}^{2}\left(F_sP_i - \dfrac{F_s}{V_m}\left(\dfrac{\mathrm{d}x_i}{\mathrm{d}t} - \dfrac{\mathrm{d}y_1}{\mathrm{d}t}\right)\right) = 0 \\ k\left(z_B - z_A - L\right) - \rho\displaystyle\sum_{i=1}^{2} O^a_{iB}\left(\dfrac{\mathrm{d}x_i}{\mathrm{d}t} - \dfrac{\mathrm{d}z_B}{\mathrm{d}t}\right) = 0 \\ k\left(z_B - z_A - L\right) + \rho\displaystyle\sum_{i=1}^{2} O^a_{iA}\left(\dfrac{\mathrm{d}x_i}{\mathrm{d}t} - \dfrac{\mathrm{d}z_A}{\mathrm{d}t}\right) = 0. \end{cases}$$

This can be reduced to

$$\begin{cases} \xi\dfrac{\mathrm{d}x_i}{\mathrm{d}t} - F_sP_i + \dfrac{F_s}{V_m}\dfrac{\mathrm{d}x_i}{\mathrm{d}t} + \rho\displaystyle\sum_{j=A,B} O^a_{ij}\dfrac{\mathrm{d}x_i}{\mathrm{d}t} = 0, \text{ for } i = 1,2 \\ \displaystyle\sum_{i=1}^{2}\left(F_sP_i - \dfrac{F_s}{V_m}\dfrac{\mathrm{d}x_i}{\mathrm{d}t}\right) = 0 \\ k\left(z_B - z_A - L\right) - \rho\displaystyle\sum_{i=1}^{2} O^a_{iB}\dfrac{\mathrm{d}x_i}{\mathrm{d}t} = 0 \\ k\left(z_B - z_A - L\right) + \rho\displaystyle\sum_{i=1}^{2} O^a_{iA}\dfrac{\mathrm{d}x_i}{\mathrm{d}t} = 0, \end{cases}$$

because symmetry causes the motor to remain in the same position ($\frac{\mathrm{d}y_1}{\mathrm{d}t} = 0$), and the stiffness of the stress fibre causes the focal adhesions to remain in approximately the same position as well ($\frac{\mathrm{d}z_{A,B}}{\mathrm{d}t} = 0$). First, we will consider the second equation. The blue filament (labelled 1), has polarity $P_1 = 1$, and the red filament (labelled 2), opposes in polarity, so $P_2 = -1$. As a result,

$$F_s - \frac{F_s}{V_m}\frac{\mathrm{d}x_1}{\mathrm{d}t} - F_s - \frac{F_s}{V_m}\frac{\mathrm{d}x_2}{\mathrm{d}t} = 0,$$

which simplifies to

$$\frac{\mathrm{d}x_1}{\mathrm{d}t} = -\frac{\mathrm{d}x_2}{\mathrm{d}t}. \tag{9}$$

This means that the two filaments are moving at the same speed but in the opposite direction. Next, if we consider the first equation for the blue filament ($i = 1$),

$$\xi\frac{\mathrm{d}x_1}{\mathrm{d}t} - F_s + \frac{F_s}{V_m}\frac{\mathrm{d}x_1}{\mathrm{d}t} + \rho\left(O^a_{1A} + O^a_{1B}\right)\frac{\mathrm{d}x_1}{\mathrm{d}t} = 0,$$

since the system is centered about the origin, the overlap between the left focal adhesion (labelled A) is given by

$$O^a_{1A} = |x_1 - l/2| = -x_1 + l/2,$$

and the right (labelled B) is given by

$$O^a_{1B} = |x_1 + l/2| = x_1 + l/2.$$

As such,

$$\xi \frac{\mathrm{d}x_1}{\mathrm{d}t} - F_s + \frac{F_s}{V_m}\frac{\mathrm{d}x_1}{\mathrm{d}t} + \rho l \frac{\mathrm{d}x_1}{\mathrm{d}t} = 0$$
$$\frac{\mathrm{d}x_1}{\mathrm{d}t} = \frac{F_s}{\xi + \frac{F_s}{V_m} + \rho l} =: V,$$

and we call this constant velocity V. From Equation 9, we obtain

$$\frac{\mathrm{d}x_2}{\mathrm{d}t} = -V$$

as the velocity of the red filament. We can hence use the third force balance equation to derive the analytical contractile force of the symmetric toy model, denoted σ.

$$\begin{aligned}\sigma(t) :&= k(z_B - z_A - L)\\ &= \rho\left(O^a_{1B}\frac{\mathrm{d}x_1}{\mathrm{d}t} + O^a_{2B}\frac{\mathrm{d}x_2}{\mathrm{d}t}\right)\\ &= \rho\left(x_1 + l/2 - (x_2 + l/2)\right)V\\ &= \rho\left(x_1 - x_2\right)V\end{aligned}$$

With the initial conditions $x_1(t=0) = -1/2$ and $x_2(t=0) = 1/2$, we determine

$$x_1 = Vt - \frac{1}{2} \text{ and } x_2 = -Vt + \frac{1}{2}.$$

Therefore,

$$\begin{aligned}\sigma(t) &= \rho\left(2Vt - 1\right)V\\ &= 2\rho V^2 t - \rho V\end{aligned}$$

is our contractile force.

8.2 Choosing Reference Parameters

This section describes how the reference parameters (given in Tables 1, 2) were chosen. For example, a grid search was performed to balance N and L. More specifically, the number of actin filaments and the length of the stress fibre was varied simultaneously. To demonstrate the effect of changing these parameters on the model's behaviour, we present Figure 25.

As seen in Figure 25b, which are trials with a longer stress fibre consisting of a smaller number of filaments, there are periods of zero contractile force. These flat periods correspond to when the stress fibre has gaps (i.e. the stress fibre is broken), and hence we would like to prevent this from occurring. When we increased the number of filaments to cover a longer stress fibre, as in Figure 25d, it reduced the occurrence of stress fibres breaking. However, 80 filaments was infeasible for the computational study, with it taking too long for the minimisers to be found. Thus, we needed

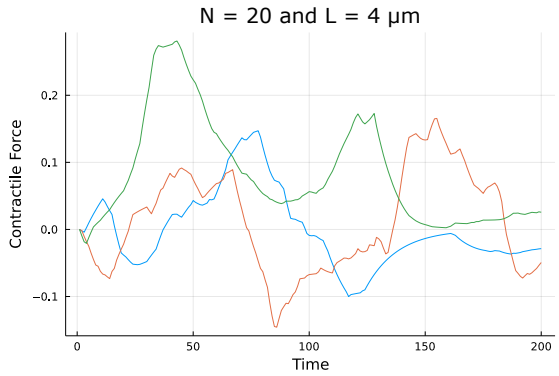

(a) Contraction of short stress fibres consisting of fewer actin filaments.

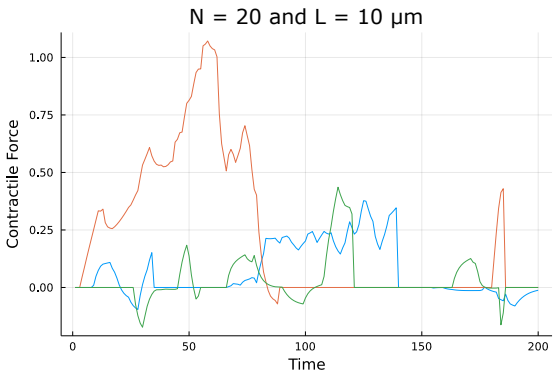

(b) Contraction of long stress fibres consisting of fewer actin filaments.

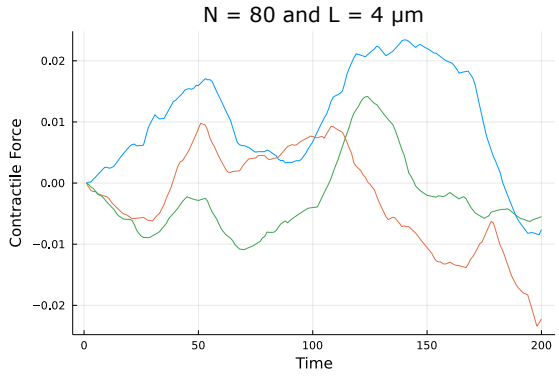

(c) Contraction of short stress fibres consisting of more actin filaments

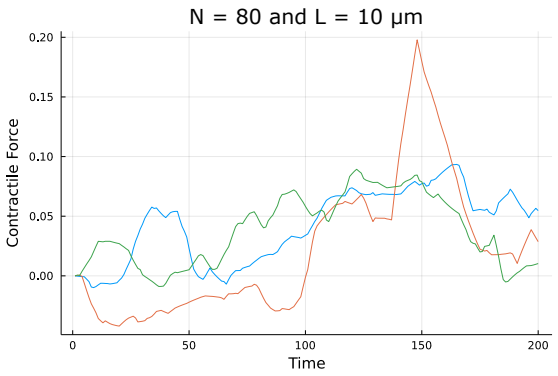

(d) Contraction of short stress fibres consisting of more actin filaments.

Figure 25: Contractile force of three stress fibres over time for various combinations of the number of filaments N and the length L of stress fibre. Each line is a separate trial with a random initial stress fibre structure.

to choose a shorter stress fibre, so that fewer filaments were necessary for the stress fibre to hold tension. There was a trade-off however. In the case of Figure 25a, with fewer filaments on a shorter stress fibre, it is more likely for there to be a heavy overlap between filaments. This causes friction to increase, which limits the movement of focal adhesions and hence the contractile force becomes weak. This relationship is exemplified by Figure 25c which, given the greater number of filaments, has contractile forces of a smaller magnitude.

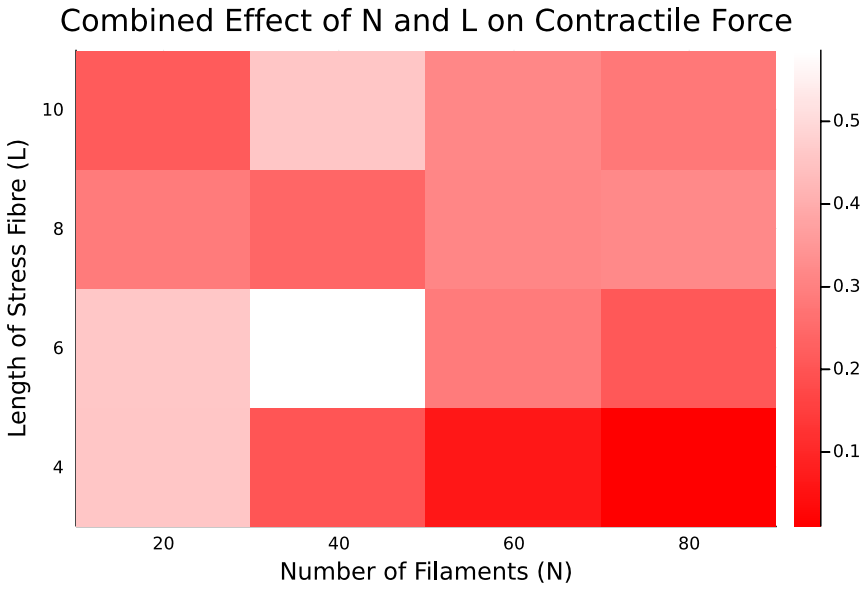

Figure 26: The mean contractile force of 10 trials with reference parameters, varying the number of filaments and the length of stress fibre.

The heat map (Figure 26) was generated to summarise this relationship, and we chose the reference stress fibre to be of length 8 µm consisting of 20 filaments. Filament bundles have been observed to have lengths between 10 to 100 µm with 4-6 filaments overlapping in one cross-section [16], so our reference parameter is pushing this minimum.

Next, we could decide on the appropriate number of motors for the reference stress fibre. For the chosen number of filaments and length of stress fibre, there was a balance between promoting stress fibre movement and complexity. Figure 27 summarises the exploration into this balance and, since reducing the number of motors reduces the expansion bias, we chose to set $M = 10$.

References

[1] Alberts, B., Johnson, A., Lewis, J., and et al. (2002). *Molecular Biology of the Cell: Blood Vessels and Endothelial Cells*. New York: Garland Science, fourth edition.

[2] Bainbridge, P. (2013). Wound healing and the role of fibroblasts. *Journal of wound care*, 22(8):407–412.

[3] Belmonte, J. M., Leptin, M., and Nédélec, F. (2017). A theory that predicts behaviors of disordered cytoskeletal networks. *Molecular Systems Biology*, 13(941).

[4] Chakraverty, S., Mahato, N. R., Karunakar, P., and Rao, T. D. (2019). *Basic Numerical Methods*, chapter 1, pages 1–17. John Wiley & Sons, Ltd.

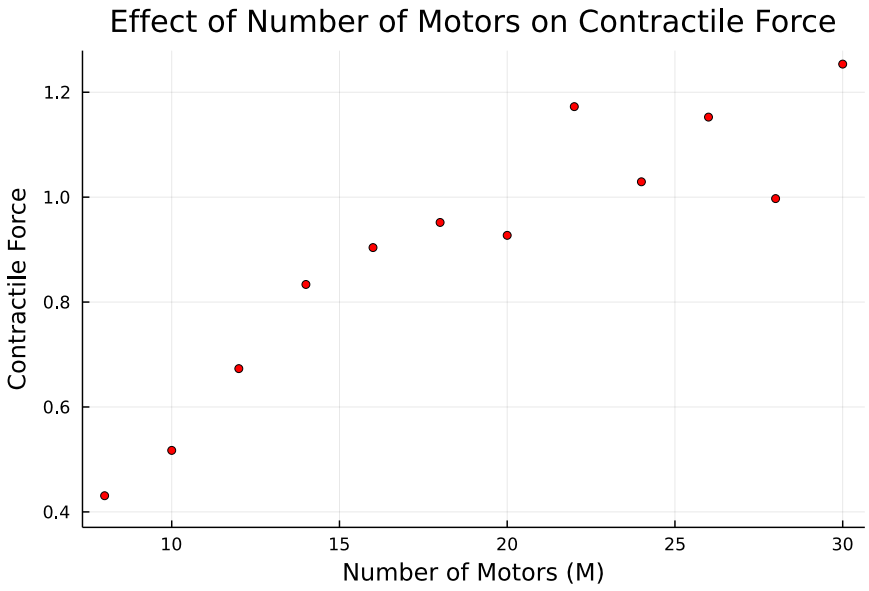

Figure 27: The mean expansive force of 10 trials with reference parameters, varying the number of motors.

[5] Charras, G. and Sahai, E. (2014). Physical influences of the extracellular environment on cell migration. *Nat Rev Mol Cell Biol*, 15:813–824.

[6] Comino, E. and Oelz, D. (2022). Actomyosin structures in stress fibres. `https://github.com/ecomino/Actomyosin-Structures-in-Stress-Fibres.git`.

[7] Encyclopaedia Britannica (2021). *Potential Energy*. Retrieved 21 October 2022 from `https://www.britannica.com/science/potential-energy`.

[8] Encyclopaedia Britannica (2022). *Energy*. Retrieved 21 October 2022 from `https://www.britannica.com/science/energy`.

[9] Frigyik, A., Srivastava, S., and Gupta, M. (2008). An introduction to functional derivatives. *UWEE Technical Report*.

[10] Gel'fand, I. M., Fomin, S. V., and Silverman, R. A. (2000). *Calculus of Variations*. Dover Books on Mathematics. Dover Publications.

[11] Hiraiwa, T. and Salbreux, G. (2016). Role of turnover in active stress generation in a filament network. *Physical Review Letters*, 116(18).

[12] Holmes, M. H. (2019). *Introduction to the Foundations of Applied Mathematics*. Texts in Applied Mathematics. Springer Cham.

[13] Komianos, J. E. and Papoian, G. A. (2018). Stochastic ratcheting on a funneled energy landscape is necessary for highly efficient contractility of actomyosin force dipoles. *Phys. Rev. X*, 8(2):021006.

[14] Lenz, M. (2014). Geometrical origins of contractility in disordered actomyosin networks. *Phys. Rev. X*, 4:041002.

[15] Lenz, M., Gardel, M. L., and Dinner, A. R. (2012a). Requirements for contractility in disordered cytoskeletal bundles. *New Journal of Physics*, 14(3):033037.

[16] Lenz, M., Thoresen, T., Gardel, M. L., and Dinner, A. R. (2012b). Contractile units in disordered actomyosin bundles arise from f-actin buckling. *Phys. Rev. X*, 108:238107.

[17] Murrell, M., Oakes, P., Lenz, M., and Gardel, M. (2015). Forcing cells into shape: the mechanics of actomyosin contractility. *Nat. Rev. Mol. Cell Biol.*, 16:486–498.

[18] Nocedal, J. and Wright, S. J. (2006). *Numerical Optimization*, chapter Large–Scale Unconstrained Optimization, pages 164–192. Springer New York, New York, NY.

[19] Oelz, D. B., Rubinstein, B. Y., and Mogilner, A. (2015). A combination of actin treadmilling and cross-linking drives contraction of random actomyosin arrays. *Biophysical Journal*, 109(9):1818–1829.

[20] Randell, S. H., Burns, K., and Boucher, R. C. (2009). Chapter 16 – epithelial cells. In Barnes, P. J., Drazen, J. M., Rennard, S. I., and Thomson, N. C., editors, *Asthma and COPD (Second Edition)*, pages 201–210. Academic Press, Oxford, second edition edition.

[21] Tam, A. K. Y., Mogilner, A., and Oelz, D. B. (2022). F-actin bending facilitates net actomyosin contraction by inhibiting expansion with plus-end-located myosin motors. *bioRxiv*.

[22] Thoresen, T., Lenz, M., and Gardel, M. L. (2011). Reconstitution of contractile actomyosin bundles. *Biophysical Journal*, 100(11):2698–2705.

[23] Tinevez, J.-Y., Schulze, U., Salbreux, G., Roensch, J., Joanny, J.-F., and Paluch, E. (2009). Role of cortical tension in bleb growth. *Biophysics and Computational Biology*, 106(44):18581–18586.

[24] Tojkander, S., Gateva, G., and Lappalainen, P. (2012). Actin stress fibers – assembly, dynamics and biological roles. *J Cell Sci*, 125(8):1855–1864.

[25] Villa, C., Chaplain, M. A. J., Gerisch, A., and Lorenzi, T. (2021). Mechanical models of pattern and form in biological tissues: The role of stress–strain constitutive equations. *Bull Math Biol*, 83(80).